International Journal of Bifurcation and Chaos

Unfolding Non-smooth Bifurcation Patterns in a 1-D PWL Map as a Model of a Single-Inductor Two-Output DC-DC Switching Converter

L. BENADERO
Departament de Física Aplicada,
Universitat Politècnica de Catalunya, Barcelona, Spain

V. MORENO-FONT
Escola Universitària Politècnica de Mataró
Fundació Tecnocampus Mataró-Maresme, Spain

A. EL AROUDI*
GAEI Research group, Departament d'Enginyeria Electrònica, Elèctrica i Automàtica,
Universitat Rovira i Virgili, Tarragona, Spain

Received on .....

A piecewise linear (PWL) continuous map is used to analyze the non-smooth bifurcation phenomena in a single-inductor two-output (SITO) DC-DC converter under a PWM interleaved control scheme. This map models the dynamical behavior of the converter when the waveforms of the inductor current can be approximated by straight lines during each switching sub-interval. The parameter space is constrained by the interleaving control and the physical restriction on the values of some parameters. The main focus of this paper is on the existence and stability conditions of the rich variety of k-periodic orbits and the different bifurcation patterns that can be exhibited in this system. The analytical results in the form of 1-D and 2-D bifurcation diagrams are compared with numerical simulations obtained from the circuit-based switched model getting a good agreement between the two approaches.

Keywords: Non-smooth Bifurcations, Chaos; Stability Analysis; Power Electronics; DC-DC converter; SITO Converter; Piecewise Linear Maps.

*Author for correspondence: e-mail: abdelali.elaroudi@urv.cat

1. Introduction

Switched mode power supplies are widely used in power management for many industrial and domestic applications due to their high efficiency, low cost and small size [Erickson and Maksimovič, 2001], [Mohan et al., 2003]. Although many switching power conversion circuits can be used, DC-DC switching converters are the most commonly used to provide an adjustable voltage/current from an unregulated voltage/current source like a photovoltaic panel or a full cell supplying a load such as an electrical machine or a microprocessor whose demanded current is changing. The simplest form of a DC-DC switching converter operates with a source supply voltage that is connected to or disconnected from the load by using switching devices like MOSFETs (controlled switches) and diodes (uncontrolled switches) and LC-filters. However, depending on the application, there are many emerging converter topologies with more complex nature. For instance, for applications where different output voltages must be stabilized to their respective references, Single-Inductor Multiple Output (SIMO) switching converter topologies are considered as a good solution [Ma et al., 2001], [Ma et al., 2003b], [Ma et al., 2003a], [Ki and Ma, 2001]. These converters make use of a single inductor and multiple switches to regulate different voltage or current levels. Hence, the desired output voltages can then be produced with higher efficiency. The presence of several switches may also allow the voltage and frequency requirements to the components to be reduced if interleaving scheme is used [Benadero et al., 2011]. However, there is a price to pay with this type of system that is obviously the added complexity that follows with the increased number of components. The switching time durations of the controlled switches are regulated via a suitable feedback to make the load voltage/current (output) as near as possible to its reference value in such a way that if the output deviates from the desired reference value, the fraction of time that the load is connected to the supplying source is increased or decreased accordingly. This switch mode operation is carried out by means of Pulse Width Modulation (PWM) action on the switches [Erickson and Maksimovič, 2001], [Mohan et al., 2003].

Like many other switched dynamical systems [Leine and Nijmeijer, 2004], DC-DC converters are highly nonlinear and may present a variety of complex dynamics that linear analysis tools generally fail to describe [El Aroudi et al., 2005], [Banerjee and Verghese, 2001], [Buti et al., 2006], [Deane and Hamill, 1990], [Deane, 1992], [Dénes and Nagy, 2003], [Banerjee, 1998], [Hamar and Nagy, 2003], [El Aroudi et al., 2000], [Kolokolov et al., 2011]. The choice of the parameter values for the switching converter and its controller strongly affect the dynamic behavior of the whole system and its stability. In addition, the presence of switches, changing

their state with time, make these kind of systems non-smooth in the sense that whenever a threshold condition is fulfilled, a switching occurs and the trajectory of the system is governed by a new set of state equations. The non-smooth trajectory will then consist of a combination of different smooth ones with each trajectory describing the smooth dynamics between two switching instants within its corresponding region of the state space. Fortunately, in the case of DC-DC converters, the system is linear during each switching interval, and the description of the continuous-time system can be then reduced to a discrete-time map that relates the state variables at the switching instants [El Aroudi et al., 2005], [El Aroudi et al., 2007]. If the switching sequence does not change, the resulting map will be smooth and the system can only present typical bifurcation phenomena like period doubling, Neimark-Sacker and Saddle-Node Bifurcations [El Aroudi et al., 2005]. However, if the switching sequence is altered, the map that results from the discretisation of the continuous-time system will be non-smooth, and it involves switching boundaries between different regions in the state space where each underlying smooth dynamics is different from the other [Yuan et al., 1998], [di Bernardo and Vasca, 2000], [di Bernardo et al., 2008], [di Bernardo et al., 1998], [Banerjee et al., 2000a], [Banerjee et al., 2000b], [Giaouris et al., 2012], [Paolini et al., 2012]. Under variation of a parameter, a fixed point of the mapping or a point of a periodic orbit may cross the boundary between two such regions leading to an abrupt change in the eigenvalues of the fixed point or periodic orbit and, hence, to a sudden change in its stability [Nusse et al., 1994], [Zhusubaliyev et al., 2003], [Zhusubaliyev et al., 2006]. The corresponding system in this case may give rise to the class of bifurcation phenomena called border-collision bifurcations that exhibit different features than their counterpart transitions that occur in smooth systems [Nusse et al., 1994]. For instance, the 2-periodic solution in a period-doubling bifurcation can be born with finite amplitude [Robert and Robert, 2002], [Robert and El Aroudi, 2006] by contrast to the parabolic growth of the 2-periodic orbit amplitude with respect to the distance to the bifurcation point observed for a conventional period doubling bifurcation [Yuan et al., 1998]. Although these phenomena have been reported in the nineties [Nusse et al., 1994], [Nusse et al., 1992], [Yuan et al., 1998], [Banerjee, 1998], a general formal mathematical approach to deal with this kind of non-smooth behavior in dynamical systems has only been available for the last few years [Zhusubaliyev et al., 2003], [Zhusubaliyev et al., 2006] [di Bernardo et al., 2008], [Leine and Nijmeijer, 2004], and more recently [Botella-Soler et al., 2012].

Smooth and non-smooth bifurcations in switching DC-DC converters, characterized by the disappearance of the desired periodic orbit under parameter variations, have been extensively studied during the two last decades, [Hamill and Jefferies, 1988] [Hamill et al., 1992], [Deane and Hamill, 1990], [Deane, 1992], [Tse, 1994], [Banerjee and Verghese, 2001], [Dénes and Nagy, 2003], [Hamar and Nagy, 2003], [El Aroudi et al., 2005], [Buti et al., 2006], [Kolokolov et al., 2011], [Tse and Li, 2011], [El Guezar et al., 2011] and [Zhang et al., 2012]. Such qualitative changes are naturally of concern to power electronics designers since they might lead to steady state solutions with different features than the desired one. Moreover, due to the non-smoothness of the descriptive Poincaré map, they may also exhibit border collision or non-smooth bifurcations [Zhusubaliyev et al., 2003], [di Bernardo et al., 1998], [Banerjee et al., 2000a], [Banerjee et al., 2000b], [Robert and Robert, 2002]. Initially, the analysis of bifurcations in the power electronic field have been mainly restricted to elementary switching converters like the buck converter in [Yuan et al., 1998] and the boost converter in [Banerjee et al., 2000b]. Later, many researchers extended their studies to more complex structures like multi-level dealt with in [Zhusubaliyev et al., 2003], [Zhusubaliyev et al., 2006] and flying capacitor multi-cell converters considered in [Robert and El Aroudi, 2006], [El Aroudi et al., 2007], paralleled converters studied in [Iu and Tse, 2000], [Iu et al., 2005], [Mazumder, 2006] and more recently cascaded converters analyzed in [Zhang et al., 2011].

Recently, we have initiated a series of studies of different nonlinear dynamic phenomena that can be exhibited by SIMO DC-DC converters with PWM. An initial stability analysis of a single inductor two-input two-output (SITO) DC-DC converter has been performed in [Benadero et al., 2006], where a single-phase control has been used, and in [El Aroudi et al., 2009] under an interleaved (two-phase) control. In [Benadero et al., 2006], the steady state properties of a single inductor two inputs two outputs SITO DC-DC converter, are first discussed and then stability is studied in terms of both power stage and control parameters by using an averaged model. In [El Aroudi et al., 2009], subharmonic oscillation and route to chaos are studied by using a discrete-time approach and a comparison between the full order model

and a simple 1-D piecewise linear (PWL) map has been carried out. In [Moreno-Font et al., 2010a], we have studied the dynamical behavior of this converter under different operating modes and with a PWM interleaved scheme, with voltage loops closed, using a discrete-time model corresponding to the main 1-periodic mode. In the same work we have shown that under certain operating conditions, the dynamical behavior of the system can be modeled by a PWL map, which was used to investigate the stability in the parameter space and to detect possible subharmonic oscillations and chaotic behavior. These results have been also confirmed by experimental measurements from a laboratory prototype. In [Moreno-Font et al., 2010b], different discrete-time models are derived and analyzed in order to describe the dynamics of SIMO switching DC-DC converters. A general procedure and further insights into the nonlinear modeling and analysis of these single-inductor DC-DC converters with multi-phase control have been presented, which is mainly focused on the formulation of maps in order to account for the different kinds of instability that these systems may exhibit and it has been shown that the 1-D PWL continuous map can reproduce most of the bifurcation phenomena predicted by the full order model in the case of a tightly regulated output voltages. Some closed form expressions for stability have been derived from this map in terms of a stability index, which is, in turn, expressed in terms of system parameters.

Our past studies have focused on the mechanisms by which the fundamental 1-periodic solution losses its stability. More recently, in [Moreno-Font et al., 2011], we have studied the formation of k-periodic orbits in the SITO converter by numerical simulations and analytically for 2-periodic orbits. This work is a step further to analyze the non-smooth behavior of the system studied in [Moreno-Font et al., 2011]. Our aim is to complete our initial study of the bifurcation processes that take place in a wide range of parameter values where the model displays a much more complicated distribution of behaviors and where new bifurcations take place. We will perform an analytical study of the non-smooth bifurcation phenomena by assuming that the output voltages of the system are regulated to their reference values. The inductor current will therefore constitute the only state variable of the system obtaining therefore a 1-D PWL continuous map with generally four domains as a dynamical model of the system. We will examine in details the conditions under which the nominal desired behavior loses its stability and we will study the patterns of its non-smooth bifurcations. First a simplified discrete-time PWL model is presented and then different scenario of bifurcation patterns are unfolded. Actually, this model is a composition of two shifted PWL maps with two pieces each and a unitary slope for the first piece. The first studied scenario is characterized by a persistence of different fixed points in which stable 1-periodic behavior is maintained. In the second scenario, chaotic orbit is born directly at the border collision bifurcation point. This scenario leads to the coexistence of the chaotic attractor and a fixed point, a result that is verified through numerical simulation from the switched circuit. The third studied scenario involves the formation of k-periodic orbits after successive border-collision period doubling bifurcations. For this scenario, the amplitude of the born periodic orbit at the bifurcation point is infinitesimal and no coexistence of orbit can take place. In the fourth scenario, the k-periodic orbits are formed through a successive period adding sequence. This scenario leads to the coexistence of attractors with different periods in some regions of the parameter space.

The rest of the paper is organized as follows: Section 2 deals with a summary description of the main features of the circuit and its switched model used for simulations. The 1-D PWL continuous map is presented in Section 3. Bifurcation patterns are discussed in Section 4 where existence and stability conditions for different k-periodic orbits ($k \geq 1$) are studied. The results are then compared, in Section 5, to those obtained from numerical simulation from the switched model. Finally, in the last section, some conclusions are presented.

2. Single-Inductor Two-Output (SITO) DC-DC converter

2.1. *Power stage circuit*

The converter under study is shown in Fig. 1. Each pair formed by the switch S_P (resp. S_N) and a diode D_P (resp. D_N) is activated in a complementary way such that when S_P (resp. S_N) is ON, D_P (resp. D_N) is OFF and vice versa. The system toggles among different configurations according to the state of the switches which are determined by the command signals u_P and u_N. For each configuration, the system equations are affine and time invariant [Moreno-Font et al., 2010a]. In order to simplify the analysis, the

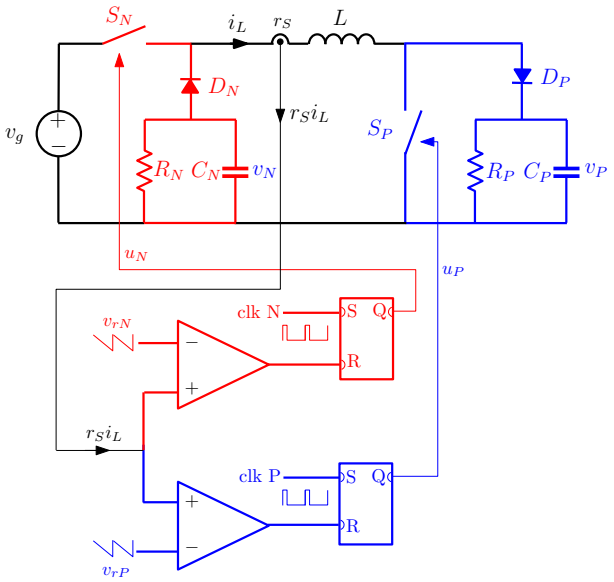

Fig. 1. Schematics circuit diagram of a SITO dc-dc converter under PWM control with current feedback.

positive and negative output voltages are considered constant, i.e, $v_P \approx V_P$ and $v_N \approx V_N$ (Fig. 2(a)). This is a practical case when for example the time constants related to the output capacitors are much greater than the switching period [Saito et al., 2007], [Kabe et al., 2007] or when the loads are simple batteries. The physical parameters are the voltage of the main source v_g, the inductance L, the output voltages (positive V_P and negative V_N).

2.2. *Current mode control of the SITO DC-DC converter*

The two main switches S_P and S_N are activated by means of a current mode control which uses two different compensating ramp signals that are compared with the control signal $r_S i_L$ in such a way that the activation of the switches is performed periodically and their turn-OFF take place whenever the control signal $r_S i_L$ intersects with one of the ramp signals. These ramps have equal amplitude V_R and period T, but different lower values V_{LP} and V_{LN}. The evolution of the inductor current during an entire period T, which is divided in two phases with durations $\phi_P T$ and $\phi_N T$ ($\phi_P + \phi_N = 1$), is represented in Fig. 2(b). The normal sequence during each of these phases corresponds to the ON state (the inductor connected to v_g) followed by the corresponding OFF state (the inductor connected to the respective load). The normal operating regime is in continuous conduction mode (CCM), with the inductor current always strictly positive, thus involving the three configurations given in Fig. 3 dictated by the state of the switches pair (S_P, S_N). The various configurations of the system take place through the binary control signals u_P and u_N that are generated at the output of the bistable flip flops and that decide the state of the switches. The correspondence of phases 1 and 2 can be arbitrarily assigned to the action on the positive and negative outputs or viceversa. Here, phase 1 is assigned to positive loading (so phase 2 corresponds to negative output). According to this choice, $\phi_1 = \phi_P$ and will be abbreviated $\phi = \phi_1$, so $\phi_2 = 1 - \phi$. During each of these phases, the converter works in a similar way than the boost converter if the positive output is concerned or the buck-boost converter when dealing with the negative output. By applying Kirchhoff's laws to the circuit depicted in Fig. 2(a), which is obtained considering tightly regulated output voltages V_N and V_P, the following differential equation is obtained

$$\frac{\mathrm{d}i_L}{\mathrm{d}t} = \frac{1}{L}\left((1-u_N)V_N + (u_P - 1)V_P + v_g u_N\right). \tag{1}$$

Strictly, other state equations are necessary to fully characterize the dynamical behavior of the system [Moreno-Font et al., 2010a]. However, considering tightly regulated output voltages, only (1) is needed [El Aroudi et al., 2009], [Moreno-Font et al., 2010b].

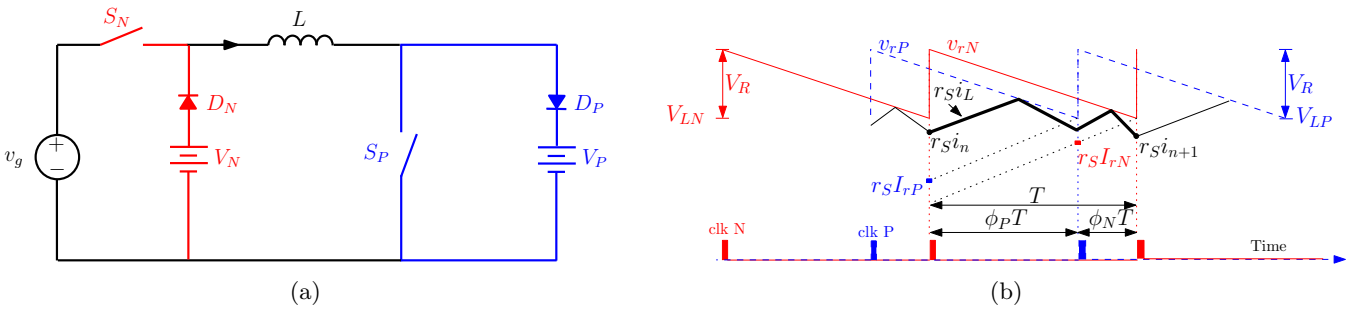

Fig. 2. (a) Simplified equivalent circuit of the power stage, (b) evolution of the relevant control signals $r_S i_L$, v_{rP} and v_{rN}.

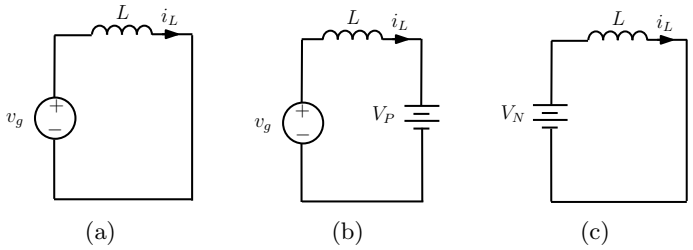

Fig. 3. Schematic circuit diagrams of the three configurations of a SITO DC-DC converter corresponding to the state of the switches pair (S_P, S_N): (a) (ON,ON), (b) (OFF,ON) and (c) (ON,OFF). The state of the diodes is always complementary to that of the switches in CCM.

3. Modeling the SITO converter by a 1-D PWL continuous map with four domains

By sampling (1) at the switching frequency, the dynamics of this converter can be modeled by means of a 1-D PWL continuous map whose unique state variable is the inductor current i_L sampled at the switching frequency [Saito et al., 2007], [Moreno-Font et al., 2011]. Moreover, the map corresponding to the SITO converter can be expressed as a composition of two sub-mappings that correspond to the two phases defined above [Moreno-Font et al., 2011]:

$$i_{n+1} = P(i_n) = P_2 \circ P_1(i_n). \tag{2}$$

Although the sub-mappings $P_1(\cdot)$ and $P_2(\cdot)$, which correspond to the first and the second phases, can be arbitrarily assigned to the action on the positive and the negative output or viceversa, the dynamics of the complete map $P(\cdot)$ is not dependent on this choice. The expressions of these sub-mappings can be easily derived, taking into account the linear time dependence of the inductor current in all configurations, therefore, obtaining the following expression for the map $P_j(\cdot)$ $(j = 1, 2)$

$$P_j(i_j) = \begin{cases} i_j + \Delta_0 \phi_j, & \text{if } i_j < I_{\gamma j} \\ I_{\gamma j} + \Delta_0 \phi_j + \lambda_j \left(i_j - I_{\gamma j}\right), & \text{if } i_j > I_{\gamma j}, \end{cases} \tag{3}$$

where $i_1 = i_L(nT)$, $i_2 = P_1(i_1)$, the current thresholds are defined as $I_{\gamma j} = I_{Lj} - \phi_j \Delta_0$, being $I_{Lj} = V_{Lj}/r_S$ (these critical values are marked in Fig. 2(b)), and

$$\lambda_j = \frac{\Delta_j - \Delta_R}{\Delta_0 - \Delta_R}. \tag{4}$$

Δ_1 and Δ_2 correspond to Δ_P and Δ_N with the choice for the order of the phases. The same criterion is applied to the other sub-indexed parameters. Parameters Δ_0, Δ_R, Δ_P and Δ_N, which are defined as current increments during the period T, are summarized in Table 1.

It can be shown from (4) and Table 1 that parameters λ_1 and λ_2 defining the slopes of the sub-mappings are both smaller than 1. In order to simplify the analysis, the map will be normalized according to the

Table 1. Incremental currents of the SITO converter.

Δ_0	$\frac{v_g}{L}T$	Δ_P	$\frac{v_g - V_P}{L}T$
Δ_R	$-\frac{V_R}{r_S}$	Δ_N	$\frac{V_N}{L}T$

following change of variable

$$x = \frac{i_1 - I_{\gamma 1}}{\Delta_0}. \tag{5}$$

Therefore, the normalized expressions of the sub-mappings $P_1(\cdot)$ and $P_2(\cdot)$ result

$$P_1(x) = \begin{cases} x + \phi, & \text{if } x < 0 \\ \lambda_1 x + \phi & \text{if } x > 0, \quad \text{and} \end{cases} \tag{6}$$

$$P_2(x') = \begin{cases} x' + 1 - \phi, & \text{if } x' < \tau + \phi \\ \lambda_2 \left(x' - \tau - \phi\right) + \tau + 1 & \text{if } x' > \tau + \phi, \end{cases} \tag{7}$$

where $x' = P_1(x)$ and

$$\tau = \frac{I_{\gamma_2} - I_{\gamma_1}}{\Delta_0} - \phi = \frac{I_{L2} - I_{L1}}{\Delta_0} - (1 - \phi).$$

The final composition of the sub-mappings ($P(x) = P_2 \circ P_1(x)$), taking into account the boundaries, gives the complete 1-D PWL continuous map in four different domains in the phase space

$$P(x) = \begin{cases} P_A(x) = x + 1, & \text{if } x \in \mathcal{D}_A = \{x \mid x < 0, \;\; x < \tau\} \\ P_B(x) = \lambda_2 x + 1 + \tau\left(1 - \lambda_2\right), & \text{if } x \in \mathcal{D}_B = \{x \mid x < 0, \;\; x > \tau\} \\ P_C(x) = \lambda_1\lambda_2 x + 1 + \tau\left(1 - \lambda_2\right), & \text{if } x \in \mathcal{D}_C = \{x \mid x > 0, \;\; \lambda_1 x > \tau\} \\ P_D(x) = \lambda_1 x + 1, & \text{if } x \in \mathcal{D}_D = \{x \mid x > 0, \;\; \lambda_1 x < \tau\}. \end{cases} \tag{8}$$

According to the definition of the domains $\mathcal{D}_i$ ($i = \{A, B, C, D\}$), a boundary Σ_{ij} between two adjacent domains $\mathcal{D}_i$ and $\mathcal{D}_j$ requires two generic conditions: one equality and an inequality to be checked. These boundaries are:

$$\Sigma_{AB} = \{x - \tau = 0, \; x < 0\}, \tag{9}$$

$$\Sigma_{BC} = \{x = 0, \; \tau < 0\}, \tag{10}$$

$$\Sigma_{CD} = \{\lambda_1 x - \tau = 0, \; x > 0\}, \tag{11}$$

$$\Sigma_{DA} = \{x = 0, \; \tau > 0\}. \tag{12}$$

It is important to notice that under the above normalization, the number of parameters is reduced to three λ_1, λ_2 and τ that stand for dimensionless slopes and the shifting between the two sub-mappings respectively. Actually, these sub-mappings are equivalent to the normalized map of a boost or buck-boost DC-DC converter under current mode control, such those considered in [Marrero et al., 1996], [Marrero et al., 1999], [Banerjee et al., 2000a], [Woywode et al., 2000] and [Woywode et al., 2001], but including a shifting between them.

According to (8), the definition of the map $P(x)$ includes four possible different domains. In order to clarify their occurrence, two diagrams in an ad-hoc mixed parameter-phase plane (τ, x) have been plotted in Fig. 4 with positive and negative sign for parameter λ_1. Note that in this representation, the domains are circular sectors and the boundaries are the splitting radii. The sectors $\mathcal{A}$ and $\mathcal{B}$, corresponding to extended domains $\mathcal{D}_A$ and $\mathcal{D}_B$ in this representation, are invariant while the sectors $\mathcal{C}$ and $\mathcal{D}$, corresponding to $\mathcal{D}_C$ and $\mathcal{D}_D$, depend on parameter λ_1.

The 1-D PWL continuous map $P(x)$ with four domains has also been represented in Fig. 5 using the four possible sign combinations for λ_1 and τ. It can be appreciated that if $\lambda_1 < 0$, the four domains appear when $\tau < 0$ (Fig. 5(a) and left side in Fig. 4(a)), but only two ($\mathcal{D}_A$ and $\mathcal{D}_D$) when $\tau > 0$ (Fig. 5(b) and

the right side in Fig. 4(a)). However, if $\lambda_1 > 0$, just three regions result, so one is excluded: $\mathcal{D}_D$ if $\tau < 0$ (see Fig. 5(c) and left side in Fig. 4(b)) or $\mathcal{D}_B$ if $\tau > 0$ (see Fig. 5(d) and the right side in Fig. 4(b))

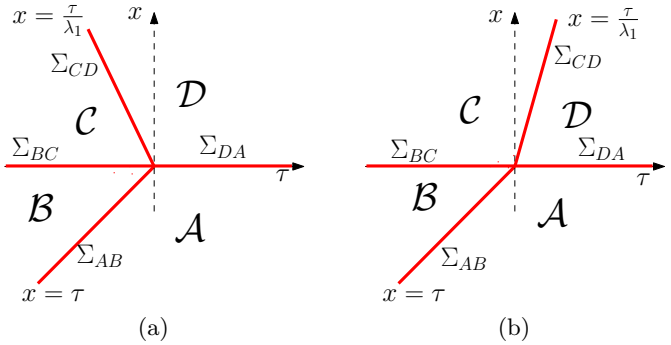

Fig. 4. Illustration of the four sectors $\mathcal{A}$, $\mathcal{B}$, $\mathcal{C}$ and $\mathcal{D}$ in the (τ, x) plane for cases (a) $\lambda_1 < 0$, (b) $\lambda_1 > 0$.

4. Analysis of the 1-D PWL map with four domains

4.1. *Normal form of PWL continuous maps with two domains. Revisited*

Let us first summarize the generic conditions of existence and stability of more complex k-periodic orbits in the form $A^{k-1}B$ for normal map $Q(x)$ with just two domains ($\mathcal{D}_A$ and $\mathcal{D}_B$) [Banerjee et al., 2000a], [di Bernardo et al., 2008]

$$Q(x) = \begin{cases} Q_A(x) = \alpha_1 x + \mu, & \text{if } x \in \mathcal{D}_A = \{x \mid x < 0\} \\ Q_B(x) = \alpha_2 x + \mu, & \text{if } x \in \mathcal{D}_B = \{x \mid x > 0\} \end{cases} \tag{13}$$

Apart from simple fixed points, k-periodic orbits type $A^{k-1}B$ (A for $\mathcal{D}_A$ and B for $\mathcal{D}_B$) can be found. The particular points of these orbits x_j^* with $j = 1 \dots k$ can be found from a set of k conditions: $Q_A(x_j^*) = x_{j+1}^*$ with $j = 1 \dots k-1$ and $Q_B(x_k^*) = x_1^*$. The sequence of these points can be expressed as

$$x_j^* = \frac{\left(1 - \alpha_1^j \left(1 - \alpha_1^{-1}\alpha_2 \left(1 - \alpha_1^{k-j}\right)\right)\right)\mu}{(1-\alpha_1)\left(1 - \alpha_1^{k-1}\alpha_2\right)}. \tag{14}$$

Similar results can be found for AB^{k-1} (due to symmetry properties of the map). Considering $A^{k-1}B$ case with $\mu > 0$ and $\alpha_1 > 0$, the orbits $A^{k-1}B$ exist if the following condition holds

$$\alpha_2 < -\frac{\alpha_1^{1-k} - 1}{\alpha_1^{-1} - 1}. \tag{15}$$

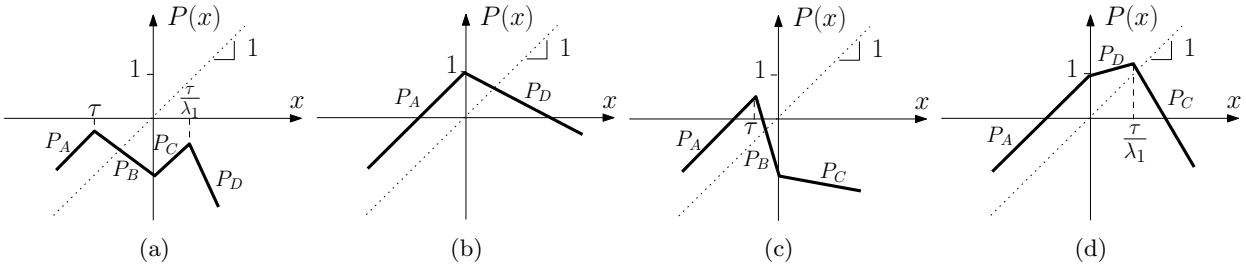

Fig. 5. Different forms of the map $P(x)$ according to the values of parameters: (a) $\{\lambda_1 < 0, \tau < 0\}$ with (A,B,C,D) partitions, (b) $\{\lambda_1 < 0, \tau > 0\}$ with (A,D), (c) $\{\lambda_1 > 0, \tau < 0\}$ with (A,B,C), and (d) $\{\lambda_1 > 0, \tau > 0\}$ with (A,D,C).

The above result is obtained by taking into account that $x^*_{j+1} = \alpha_1 x^*_j + \mu$ (if $j = 1 \dots k-1$), so it is only necessary to impose membership condition for $k-1$ fixed point ($x^*_{k-1} \in \mathcal{D}_A : \; x^*_{k-1} < 0$). Finally, due to the piecewise linearity of the map, the orbits $A^{k-1}B$ are stable provided that the following condition holds

$$\mid \alpha_1^{k-1}\alpha_2 \mid < 1. \tag{16}$$

4.2. *Symmetry in the parameter space*

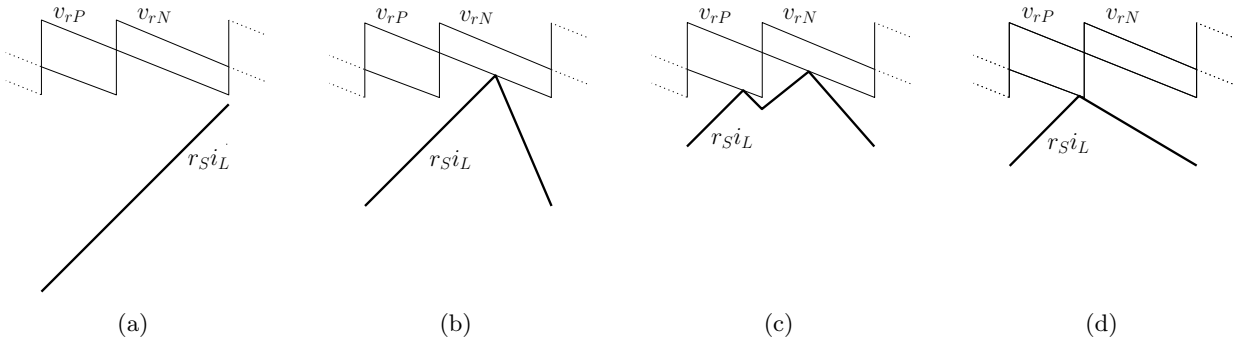

Fig. 6. The ramp signals v_{rP} and v_{rN} and the control signal $r_S i_L$ waveforms for cases: $NN \equiv A$ in (a), $NY \equiv B$ in (b), $YY \equiv C$ in (c), and $YN \equiv D$ in (d).

The dynamics generated by the map $P(x)$ defined in (8) alternates the two subintervals that are associated to both phases. Periodic orbits can then be described by symbolic sequences of a pair of elements, each of them related to one phase. These elements can be of two different types, which will be denoted here Y and N according to the presence (Y) or absence (N) of an asynchronous switching during the corresponding phase. To be precise, Y means a sequence ON-OFF during the associated phase, while in case N, the ON topology is the only one given. The first symbol (either Y or N) and, in general, symbols placed in odd position will correspond to phase 1, while symbols placed in an even position will correspond to phase 2. Actually, this notation highlights the fact that the map is formed by the composition of the two sub-mappings.

In Fig. 6, the four simplest sequences of subintervals NN, NY, YY and YN are represented. They will be abbreviated in accordance to items in (8) (A, B, C and D respectively). It should be noticed that, with appropriate parameter values, only B, C and D cases can correspond to 1-periodic orbits, whereas A cannot be a periodic orbit. Possible 2-periodic orbits correspond to the following sequences of subintervals: $NNNY$, $NNYN$, $NNYY$, $NYYN$, $NYYY$ and $YYYN$ (in short form: ab, ad, AC, BD, BC and CD respectively). Note that periodic orbit sequences cannot contain subsequences formed by a unique symbol (for example, C^2) due to the linearity of the map within each domain. Lower case letters will be used (for instance, ab and ad), in some cases for those orbits that are unstable.

Taking into account that the selected order of phases is purely arbitrary, if that order were inverted, the (Y, N) symbol sequence should be shifted one step or in general an odd number of steps, because even shifting produces no change. Obviously, if the phase order is inverted, parameters λ_1 and λ_2 must be interchanged and the parameter τ must be changed to $-1-\tau$.

Under the inversion of the phase order, orbits like NY, YY or YN will result as YN, YY or NY respectively or in the abbreviated form B, C and D are equivalent to D, C and B respectively. Dealing with 2-periodic orbits, ab, ad, AC, BD, BC and CD will be renamed as ad, ab, BD, AC, CD and BC respectively. For the purpose of this paper, symmetry will be used to simplify the analysis. Consequently, properties (i.e., existence and stability) of periodic orbits like D, ab, BD or CD are equivalent to B, ad, AC or BC respectively, in the understanding that parameters must be changed in accordance to the rules described above (λ_1 by λ_2 and vice versa and τ by $-1-\tau$). These facts will be taken into account to plot the bifurcation diagrams.

4.3. *Existence of the fixed points*

The 1-D PWL continuous map can have up to three[1] kind of fixed points. Moreover, some of them can coexist depending on the range of the parameters of the map. These fixed points $x_j^*(\, j \in \{B, C, D\})$ are solutions of the equation $P_j(x_j^*) = x_j^*$, so they must be located inside the corresponding domain (that is $x_j \in \mathcal{D}_j$) in order to be admissible or real. On the contrary, a fixed point is called non admissible or virtual if it is not in the domain of existence. These points will be excluded in the analysis. The expressions of the fixed points in the regions $\mathcal{D}_B$, $\mathcal{D}_C$ and $\mathcal{D}_D$ are

$$x_B^* = \frac{1}{1-\lambda_2} + \tau, \quad x_C^* = \frac{1+\tau\,(1-\lambda_2)}{1-\lambda_1\lambda_2}, \quad x_D^* = \frac{1}{1-\lambda_1}.$$

4.3.1. *Fixed point in the domain $\mathcal{D}_B$*

Imposing that the fixed point $x_B \in \mathcal{D}_B$, it will exist if

$$x_B^* < 0 \quad \text{and} \quad x_B^* > \tau. \tag{17}$$

The second condition in (17) is always fulfilled because $\lambda_2 < 1$, and the first condition can be expressed as

$$\tau < -\frac{1}{1-\lambda_2} \equiv \tau_{B\leftrightarrow C}. \tag{18}$$

where $\tau_{B\leftrightarrow C}$ is the critical value of τ at which the fixed point x_B^* collides with the border Σ_{BC} and with the fixed point x_C^*.

4.3.2. *Fixed point in the domain $\mathcal{D}_D$*

The existence of x_D^* is determined by the conditions

$$x_D^* > 0 \quad \text{and} \quad \lambda_1 x_D^* < \tau. \tag{19}$$

The first condition in (19) is also fulfilled because $\lambda_1 < 1$. Therefore, from the second condition, the fixed point x_D^* exists if the following inequality holds

$$\tau > \frac{\lambda_1}{1-\lambda_1} \equiv \tau_{C\leftrightarrow D}, \tag{20}$$

where, as before, $\tau_{C\leftrightarrow D}$ corresponds to the collision between the fixed points x_C^* and x_D^* and their corresponding boundary Σ_{CD}. Notice that

$$\tau_{C\leftrightarrow D} - \tau_{B\leftrightarrow C} = \frac{1-\lambda_1\lambda_2}{(1-\lambda_1)\,(1-\lambda_2)}.$$

Therefore, $\tau_{B\leftrightarrow C} < \tau_{C\leftrightarrow D}$ if $\lambda_1\lambda_2 < 1$. Otherwise, if the slopes product $\lambda_1\lambda_2 > 1$, one has $\tau_{C\leftrightarrow D} < \tau_{B\leftrightarrow C}$.

4.3.3. *Fixed point in the domain $\mathcal{D}_C$*

Dealing with the fixed point x_C^*, firstly note that this point becomes singular when the slopes product $\lambda_1\lambda_2 = 1$. The existence conditions are

$$x_C^* > 0 \quad \text{and} \quad \lambda_1 x_C^* > \tau. \tag{21}$$

From (21), one can conclude that: 1) if the slopes product $\lambda_1\lambda_2 < 1$, x_C^* exists if $\tau_{B\leftrightarrow C} < \tau < \tau_{C\leftrightarrow D}$ (in this case one and only one fixed point is admissible: x_B^* if $\tau < \tau_{B\leftrightarrow C}$, x_D^* if $\tau_{C\leftrightarrow D} < \tau$ or x_C^* for the intermediate values of τ); 2) if $\lambda_1\lambda_2 > 1$, x_C^* exists if $\tau_{C\leftrightarrow D} < \tau < \tau_{B\leftrightarrow C}$ (indeed, all fixed points x_B^*, x_C^* and x_D^* are simultaneously admissible in this parameter region).

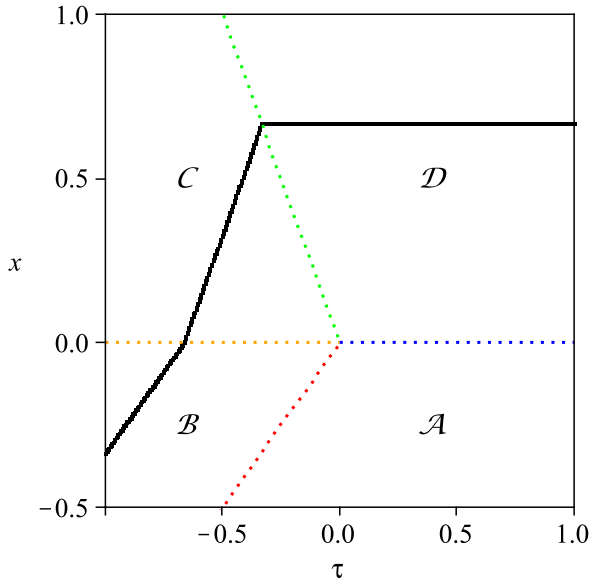

Fig. 7. Numerically obtained bifurcation diagram taking τ as a bifurcation parameter with the fixed parameters $\lambda_1 = \lambda_2 = -0.5$, such that fixed points are all stable. To highlight the sectors, the existence boundaries are also plotted.

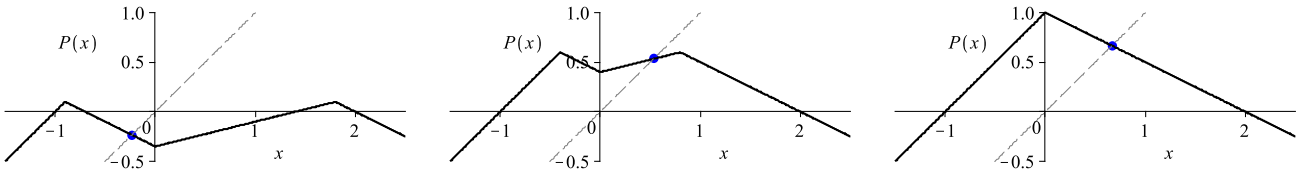

(a) (b) (c)

Fig. 8. The map $P(x)$ with fixed parameters as in Fig. 7 and (grey dashed) unitary slope line intersect at the fixed points (a) x_B^* (with $\tau = -0.9$), (b) x_C^* ($\tau = -0.4$) and (c) x_D^* ($\tau = 0.1$). Notice that in (c) only $P_A(x)$ and $P_D(x)$ apply since $\tau > 0$ and $\tau/\lambda_1 < 0$.

4.4. *Stability of the fixed points and illustrative cases*

The stability analysis can be carried out directly from the derivatives of $P_j(x)$. Due to the linearity of the map within each domain, the stability condition of the fixed points x_B^*, x_C^* or x_D^* is guaranteed if (in addition to the parameter restrictions $\lambda_1 < 1$ and $\lambda_2 < 1$) $\lambda_2 > -1$, $|\lambda_1\lambda_2| < 1$ or $\lambda_1 > -1$ respectively. Notice that if $\lambda_1\lambda_2 > 1$, x_C^* and at least one of the other points (x_B^* or x_D^*) is unstable, so at most one fixed point (x_B^* or x_D^*) can be stable.

The bifurcation diagram in Fig. 7, which has been obtained by numerical simulation with appropriate parameters, shows persistence between the three stable fixed points. A representative point for each case

[1]Note that in the domain $\mathcal{D}_A$, no fixed point exists because the slope of the map in this region is 1 and the map does not cross the origin.

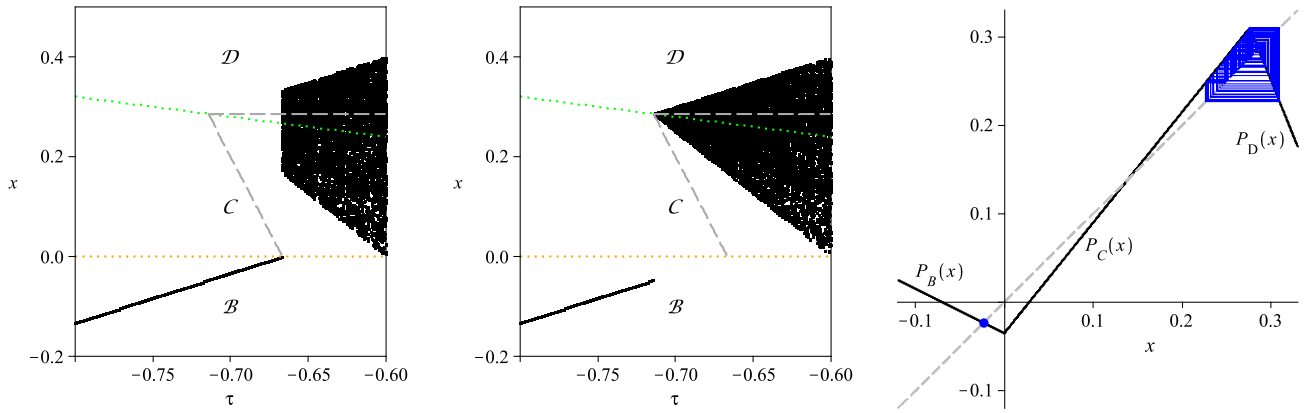

Fig. 9. Numerically obtained bifurcation diagrams calculated by sweeping the bifurcation parameter τ from (a) left to right and (b) right to left. The grey dashed lines accounting for unstable x_C^* and x_D^* and the existence boundaries are also included. (c) cobweb diagram with $\tau = -0.69$ to show the coexistence of fixed point x_B^* with a chaotic dynamic constrained in domains $\mathcal{D}_C$ and $\mathcal{D}_D$. The unstable fixed point (x_C^*) is a boundary of their basins. The fixed parameters used here ($\lambda_1 = -2.5$ and $\lambda_2 = -0.5$) are such that only fixed point x_B^* is stable within its domain of existence.

is given in Fig. 8, where fixed points correspond to the intersection of the map $P(x)$ with the unitary slope straight line.

The diagrams in Fig. 9(a) and Fig. 9(b) have been computed at a different parameter region, such that only fixed point x_B^* (if admissible) is stable. Both diagrams use the same parameters, but the bifurcation parameter τ is swept from left to right in the diagram on the left and in the opposite direction in the other diagram. It can be appreciated a chaotic dynamic that emerges at the bifurcation point $\tau_{C\leftrightarrow D}$ and it coexists with the fixed point x_B^* as long as it is admissible (until the bifurcation point $\tau_{B\leftrightarrow C}$). The stable fixed point x_B^*, given by the intersection of $P_B(x)$ and the unitary slope line, and the chaotic attractor, with points belonging to the domains $\mathcal{D}_C$ and $\mathcal{D}_D$, are observed in the cobweb plot in Fig. 9(c). Notice that $P_C(x)$ intersects the unitary slope line at the unstable fixed point x_C^* that is in fact the boundary between the basins of the attractions of the two attractors. It can also be observed that the chaotic behavior is robust with no periodic windows [Banerjee, 1998] and that the attractor itself is bounded by two points related to Σ_{CD}. These are $P(\tau/\lambda_1) = 1 + \tau$ and $P^2(\tau/\lambda_1) = 1 + \lambda_1(1 + \tau)$.

4.5. *Divergence analysis*

Before going further to analyze 2-periodic orbits and more complex k-periodic orbits, we will demonstrate that the dynamics of the 1-D PWL continuous map $P(x)$ cannot diverge with our restrictions in the physical parameters ($\lambda_1 < 1$ and $\lambda_2 < 1$). Considering the form of $P_A(x)$, divergence is only possible in the positive side of the phase space ($x \to +\infty$), which corresponds to either domain $\mathcal{D}_C$ or $\mathcal{D}_D$. Divergence implies a positive slope and larger than 1 in the corresponding domain ($\lambda_1\lambda_2 > 1$ or $\lambda_1 > 1$ for $P_C(x)$ or $P_D(x)$ in domains $\mathcal{D}_C$ or $\mathcal{D}_D$ respectively). Divergence involving domain $\mathcal{D}_C$ implies $\lambda_1 > 0$, thus requiring $\lambda_2 > 0$ in order to fulfill the divergence condition $\lambda_1\lambda_2 > 1$ and in addition, at least λ_1 or λ_2 should be larger than 1. Because these parameters are smaller than 1 with our physical restrictions, divergence is not possible in this case. Divergence involving the domain $\mathcal{D}_D$ (given with $\lambda_1 < 0$) and its respective divergence condition ($\lambda_1 > 1$) are mutually contradictory, so divergence is also impossible.

The final conclusion is that divergence is only possible with $\lambda_1 > 0$, $\lambda_2 > 0$ and $\lambda_1\lambda_2 > 1$ and this set of conditions requires that at least $\lambda_1 > 1$ or $\lambda_2 > 1$, thus violating the physical restrictions.

4.6. *2-periodic orbits*

As it is well known, different scenarios are possible in PWL continuous maps when fixed points become unstable [Banerjee et al., 2000a], [Banerjee et al., 2000b]. Regarding the 1-D PWL continuous map $P(x)$,

Table 2. Different 2-periodic orbits.

$x^*_{AB} = \dfrac{1+\lambda_2}{1-\lambda_2} + \tau$ $x^*_{BA} = \dfrac{2}{1-\lambda_2} + \tau$	$x^*_{AC} = \dfrac{(1+\lambda_1\lambda_2) + \tau\,(1-\lambda_2)}{1-\lambda_1\lambda_2}$ $x^*_{CA} = \dfrac{2+\tau\,(1-\lambda_2)}{1-\lambda_1\lambda_2}$	$x^*_{BC} = \dfrac{(1+\lambda_1\lambda_2)\,(1+\tau\,(1-\lambda_2))}{1-\lambda_1\lambda_2^2}$ $x^*_{CB} = \dfrac{(1+\lambda_2)\,(1+\tau\,(1-\lambda_2))}{1-\lambda_1\lambda_2^2}$
$x^*_{AD} = \dfrac{1+\lambda_1}{1-\lambda_1}$ $x^*_{DA} = \dfrac{2}{1-\lambda_1}$	$x^*_{BD} = \dfrac{(1+\lambda_1) + \tau\lambda_1\,(1-\lambda_2)}{1-\lambda_1\lambda_2}$ $x^*_{DB} = \dfrac{(1+\lambda_2) + \tau\,(1-\lambda_2)}{1-\lambda_1\lambda_2}$	$x^*_{CD} = \dfrac{(1+\lambda_1) + \tau\lambda_1\,(1-\lambda_2)}{1-\lambda_1^2\lambda_2}$ $x^*_{DC} = \dfrac{(1+\lambda_1\lambda_2) + \tau\,(1-\lambda_2)}{1-\lambda_1^2\lambda_2}$

only k-periodic ($k > 1$) orbits or chaotic dynamics can be exhibited if divergence cannot occur as it is the case considered in this study. Actually, chaos will be the response of the system in those cases that periodic orbits are unstable as it the case of Fig. 9. In this and following sections, the existence and stability of 2-periodic and later some higher periodic orbits will be investigated.

The expressions of the fixed points belonging to the full set of possible 2-periodic orbits (i.e., the six pair combinations of the four domains of the map) that are obtained by equations of the form $P_j(P_i(x^*_{ij})) = x^*_{ij}$ (being $x^*_{ji} = P_i(x^*_{ij})$) are summarized in Table 2. The existence and stability conditions of each of these orbits are addressed below.

4.6.1. *The orbits AB/ab and AD/ad*

The orbit AB/ab, and in general any orbit including the domain $\mathcal{D}_B$, cannot exist for positive values of τ. In addition to the constraint $\tau < 0$, the existence conditions of these orbits are $x^*_{AB} < \tau \quad \text{and} \quad \tau < x^*_{BA} < 0$. From these inequalities and taking into account the parameter restriction $\lambda_2 < 1$, the orbit AB/ab exists if $\lambda_2 < -1$ and

$$\tau < -\frac{2}{1-\lambda_2} \equiv \tau_{AB\leftrightarrow AC}. \tag{22}$$

The critical value $\tau_{AB\leftrightarrow AC}$ corresponds to the collision between the fixed points x^*_{BA} and x^*_{CA} and their corresponding boundary Σ_{BC}.

Applying the conditions of symmetry (replacing λ_2 and τ by λ_1 and $-(1+\tau)$), the orbit AD/ad can only exist if $\lambda_1 < -1$ and, from (22), also if

$$\tau > \frac{1+\lambda_1}{1-\lambda_1} \equiv \tau_{AD\leftrightarrow BD}. \tag{23}$$

Similarly, $\tau_{AD\leftrightarrow BD}$ corresponds to the collision between the fixed points x^*_{AD} and x^*_{BD} and their corresponding boundary Σ_{AB}. The stability conditions for both orbits imply $|\lambda_2| < 1$ and $|\lambda_1| < 1$ respectively and therefore, they are always unstable.

To sum up, unstable orbit ab (or ad) exists if $\lambda_2 < 1$ (or $\lambda_1 < 1$) and $\tau < \tau_{AB\leftrightarrow AC}$ (or $\tau_{AD\leftrightarrow BD} < \tau$). This condition involves a border collision at boundary Σ_{BC} (or Σ_{AB}), thus implying a transition to the orbit AC/ac (or BD/bd) that will be analyzed bellow.

4.6.2. *The orbits AC/ac and BD/bd*

The orbit AC/ac as well as ab, from which is generated, requires the condition $\lambda_2 < -1$ and shares the same limit $\tau_{AB\leftrightarrow AC}$. An additional critical value of τ is related to the point of the 2-periodic orbit in the domain $\mathcal{D}_A$, thus concerning the boundaries Σ_{AB} or Σ_{AD}.

$$\tau_{AC\leftrightarrow BC} \equiv \frac{1+\lambda_1\lambda_2}{\lambda_2\,(1-\lambda_1)}, \tag{24}$$

$$\tau_{AC\leftrightarrow DC} \equiv -\frac{1+\lambda_1\lambda_2}{1-\lambda_2}. \tag{25}$$

The orbits AC and BD are stable if $|\lambda_1\lambda_2| < 1$. Moreover, $\lambda_1\lambda_2$ determines three different existence ranges.

Concerning AC, if $\lambda_1\lambda_2 > 1$ (so the orbit is unstable), the derivative of the fixed points with respect to the parameter τ is negative, giving the range $\tau_{AC\leftrightarrow BC} < \tau < \tau_{AB\leftrightarrow AC}$. Alternatively, if $\lambda_1\lambda_2 < 1$, the condition $\tau_{AB\leftrightarrow AC} < \tau$ must be fulfilled, with two additional subcases: if $-1 < \lambda_1\lambda_2 < 1$ (therefore the orbit is stable), the valid boundary is Σ_{AB} so the range to be applied is $\tau_{AB\leftrightarrow AC} < \tau < \tau_{AC\leftrightarrow BC}$. Otherwise, if $\lambda_1\lambda_2 < -1$ (the orbit is then unstable), the valid boundary is Σ_{AD} corresponding to the range $\tau_{AB\leftrightarrow AC} < \tau < \tau_{AC\leftrightarrow DC}$.

Taking into account the symmetry, the existence conditions of the orbit BD/bd are $\lambda_1 < -1$ and: $\tau_{AD\leftrightarrow BD} < \tau < \tau_{BD\leftrightarrow CD}$ if $\lambda_1\lambda_2 > 1$, $\tau_{BD\leftrightarrow CD} < \tau < \tau_{AC\leftrightarrow BC}$ if $-1 < \lambda_1\lambda_2 < 1$ or $\tau_{BD\leftrightarrow BC} < \tau < \tau_{AC\leftrightarrow BC}$ if $\lambda_1\lambda_2 < -1$, where

$$\tau_{BD\leftrightarrow CD} \equiv -\frac{1+\lambda_1}{\lambda_1\,(1-\lambda_2)}, \tag{26}$$

$$\tau_{BD\leftrightarrow BC} \equiv -\frac{\lambda_1\,(1+\lambda_2)}{1-\lambda_1}. \tag{27}$$

4.6.3. *The orbits BC/bc and CD/cd*

The orbit BC/bc is stable if $\mid \lambda_1\lambda_2^2 \mid < 1$ and it exists under anyone of the following set of conditions:

- $\lambda_2 < -1$, $\lambda_1\lambda_2 > -1$ and either $\tau_{B\leftrightarrow C} < \tau < \tau_{AC\leftrightarrow BC}$ if $\lambda_1\lambda_2^2 > 1$ which correspond to the unstable case or $\tau_{AC\leftrightarrow BC} < \tau < \tau_{B\leftrightarrow C}$ otherwise.
- $\lambda_2 > -1$, $\lambda_1\lambda_2 < -1$ and $\lambda_1\lambda_2^2 < 1$ in addition to $\tau_{B\leftrightarrow C} < \tau < \tau_{BC\leftrightarrow BD}$.

Taking into account the symmetry, the orbit CD/cd is stable if $\mid \lambda_1^2\lambda_2 \mid < 1$ and it exists under the following conditions:

- $\lambda_1 < -1$, $\lambda_1\lambda_2 > -1$ and either $\tau_{BD\leftrightarrow CD} < \tau < \tau_{C\leftrightarrow D}$ if $\lambda_1^2\lambda_2 > 1$ (in this case it is unstable) or $\tau_{C\leftrightarrow D} < \tau < \tau_{BD\leftrightarrow CD}$ otherwise.
- $\lambda_1 > -1$, $\lambda_1\lambda_2 < -1$ and $\lambda_1^2\lambda_2 < 1$ together with $\tau_{B\leftrightarrow C} < \tau < \tau_{AC\leftrightarrow DC}$.

4.6.4. *Examples and discussion on 2-periodic orbits*

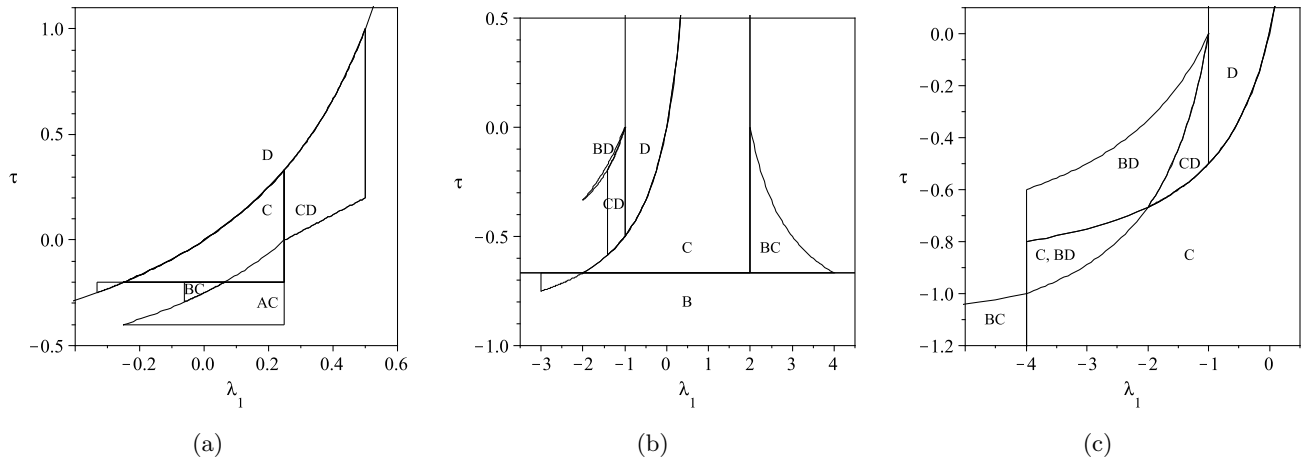

Fig. 10. Bifurcation diagrams for stable 1-periodic and 2-periodic orbits obtained analytically. The parameter values are: (a) $\lambda_2 = -4$, (b) $\lambda_2 = -0.5$ and (c) $\lambda_2 = 0.25$.

In order to illustrate some of the results derived for 2-periodic orbits, three analytically obtained 2-D bifurcation diagrams in the parameter plane (λ_1, τ) with fixed parameter $\lambda_2 = -4$ in Fig. 10(a), $\lambda_2 = -0.5$ in Fig. 10(b) and $\lambda_2 = 0.25$ in Fig. 10(c) have been represented. The diagram in Fig. 10(a) meets conditions

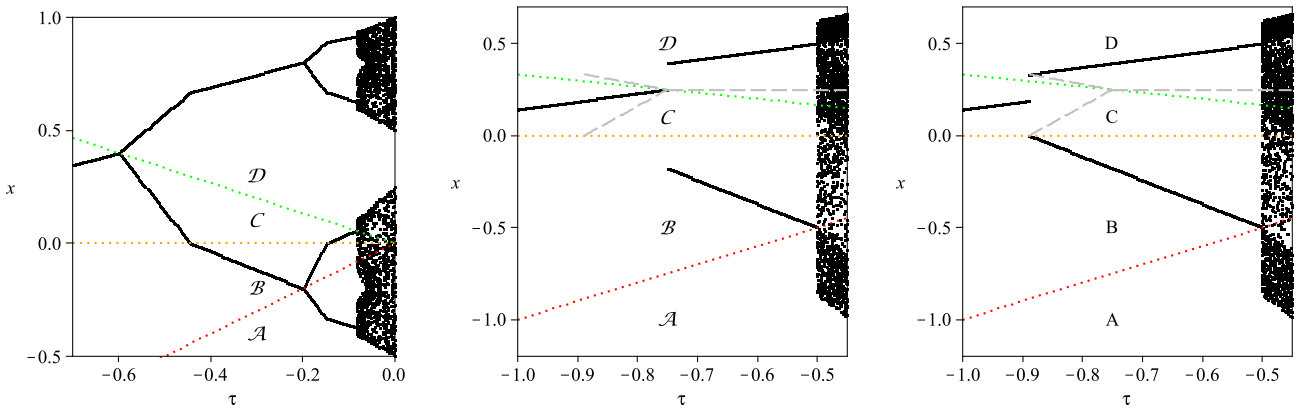

Fig. 11. Bifurcation diagrams and existence boundaries by varying parameter τ with $\lambda_2 = 0.25$ (so they are sections in Fig. 10(c)) and $\lambda_1 = -1.5$ in (a) and $\lambda_1 = -3$ in (b) and (c) (the unstable fixed point x_D^* is also plotted). These last two diagrams have been calculated from left to right in (b) or from right to left in (c) and the grey dashed lines for the unstable *cd* orbit have been included in order to explain the observed multi-stability (coexistence of C and BD periodic orbits).

for stable orbits D, C, AC, BC and CD, and diagram in Fig. 10(b) does for B, C, D, BC, CD and BD. In diagram in Fig. 10(b), the inclusion of the chaotic region inside region B that can be observed is due to the continuation of the existence curve for the fixed point x_C^*. Actually, the bifurcation diagrams in Fig. 9 have been computed across this region of coexistence. A similar inclusion of a chaotic regime appears on the bottom-left side of region D in Fig. 10(a) that is also related to the existence of the unstable fixed point x_C^*.

Some extra 1-D bifurcation diagrams have been computed across sections in Fig. 10(c). The diagram in Fig. 11(a) is obtained by selecting $\lambda_1 = -1.5$ showing perfect matching for the existence limits of C, CD and BD orbits obtained analytically. In the transition from C to d, the eigenvalues jump from $\lambda_1\lambda_2 = -0.375$ to $\lambda_1 = -1.5 < -1$. This transition cannot correspond to a persistence border collision bifurcation at Σ_{CD}. Analyzing the existing periodic orbit CD, it is found that it is stable according to the corresponding eigenvalues $\lambda_1^2\lambda_2 = 0.5625$, so there is a non-smooth supercritical flip or period doubling bifurcation. Unlike that case, there is persistence from CD to BD at Σ_{BC} because the eigenvalue of BD is within the unit circle ($-1 < \lambda_1\lambda_2 = -0.375 < 1$). Furthermore, this diagram shows the presence of more complex orbits: another non-smooth period doubling bifurcation from BD to $ADBD$ at Σ_{AB} (due to unstable *ab* with eigenvalue $\lambda_1 = -1.5 < -1$) and persistence from $ADBD$ to $ADCD$ at Σ_{BC}. Finally there is a direct transition to chaos at the collision with Σ_{CD} ($ADCD$ to *addd* with unstable eigenvalue $\lambda_1^3 = -2.8125 < -1$). All features for these new orbits can be demonstrated following a similar procedure to that for 2-periodic orbits.

It is interesting to notice here that sequences of orbits similar to the described above are found throughout the parameter space. The idea is that in general from an existing stable orbit, a new one can emerge in its limit of existence, either by persistence or period doubling. From the new orbit the same process can be repeated and so on. The orbits are therefore increasingly complex until chaos is reached. Unlike the smooth counterpart (i.e, the period doubling route to chaos in a logistic or similar map), this sequence is finite, so abruptly leading to chaotic oscillation when no more stable orbits exist. Regarding the diagram in Fig. 11(a), after $ADCD$ limit at Σ_{CD} boundary, besides unstable *addd*, emerging period doubling orbit $ADCDADDD/adcdaddd$ is also unstable because its corresponding eigenvalue is $\lambda_1^6\lambda_2 = 2.85 > 1$, thus giving rise to chaos.

In order to show a common pattern in the formation of multi-stability, let us show another two bifurcation diagrams using also a section in Fig. 10(c), but with $\lambda_1 = -3$. Apart from the numerical results, and in order to make more comprehensive the analysis, the analytical results for the fixed points of the unstable 1-periodic orbit d (with eigenvalue $\lambda_1 = -3 < -1$) and the unstable 2-periodic orbit

cd (with eigenvalue $\lambda_1^2\lambda_2 = 2.25 > 1$) have also been depicted. The diagram in Fig. 11(b) has been performed by increasing the parameter τ (from left to right), thus showing how the former orbit C, with eigenvalue $\lambda_1\lambda_2 = -0.75$, links to cd at Σ_{CD}. The complete local bifurcation scheme corresponds to the transition $\{C, cd\} \leftrightarrow \{d\}$, which is in fact a non-smooth subcritical period doubling bifurcation. One can notice, in this case, that the eigenvalue of d is $\lambda_1 = -3 < -1$. The diagram in Fig. 11(c), plotted by decreasing the parameter τ (right to left) helps to understand the global behavior. It can be appreciated a local non-smooth fold bifurcation at Σ_{BC} in the form $\{BD, cd\} \leftrightarrow \{\emptyset\}$. Recall that cd has an eigenvalue $\lambda_1^2\lambda_2 = 2.25 > 1$ and the BD eigenvalue is $\lambda_1\lambda_2 = -0.75$. The result is the coexistence of C and BD in the range $\tau_{BD\leftrightarrow CD} < \tau < \tau_{C\leftrightarrow D}$, being $\tau_{BD\leftrightarrow CD} = -0.8889$, $\tau_{C\leftrightarrow D} = -0.75$, where a perfect matching can be appreciated between analytical and numerical methods. Finally, chaos emerges when BD collides the boundary Σ_{AB}.

The coexistence of attractors is also found for C and AC (Fig. 10(a)). As this case is common for orbits of type $A^{k-1}C$, it will be analyzed in the following section, which is dedicated to some series of high periodic orbits. Before dealing with them, we would like to emphasize the fact that in PWL continuous maps like $P(x)$, a k-periodic orbit can emerge after a bifurcation (period doubling is the particular case for $k = 2$). The general idea is that from a former orbit say X (X being a sequence with several partitions, for instance $X = AC$), an orbit type $X^{n-1}Y$ (n is an integer > 1) can emerge with appropriate parameters, Y being equivalent to X except for the partition that take place at the bifurcation boundary. For instance, with convenient parameters, after the former orbit AC collides with the boundary Σ_{BC}, an orbit of the type $ABACAC$ can possibly emerge. In this example we have chosen $X = AC$, $Y = AB$, and $n = 3$. The orbits $B^{k-1}C$, CD^{k-1} and BC^{k-1} that will be analyzed below are particular cases of emerging multiple period orbits after a non smooth bifurcation.

4.7. *k-periodic orbits*

Apart from 1-periodic and 2-periodic orbits, there are many more complex k-periodic orbits with higher periodicity ($k > 2$) that can be observed in the numerical simulations. In general, a variety of domains are involved in these orbits and they appear under certain grouping patterns in bifurcation diagrams in a suitable parameter space. The periodic orbits involving only two domains, among the four possible, will be analyzed in detail in this paper, starting by those of the generic form $B^{k-1}C$. In the 2-D analytically obtained bifurcation diagrams and other parts of the text, the orbits $B^{k-1}C$ will appear as $\underbrace{BB\ldots B}_{k-1 \text{ times}}C$ and the same apply for other orbits.

4.7.1. *The series of type $B^{k-1}C/b^{k-1}c$*

Orbits $B^{k-1}C/b^{k-1}c$ are k-periodic and equivalent to CD^{k-1}/cd^{k-1} if the order of phases is inverted. Each member of the series $B^{k-1}C/b^{k-1}c$ can emerge after a border collision of a stable 1-periodic orbit type B, so all these orbits are merged to B in the parameter space, when the parameter τ is varied. The 2-D bifurcation diagram in the parameter space (λ_1, τ) in Fig. 12(a) illustrates the case for $\lambda_2 = 0.25$. The particular cases C ($k = 1$) and BC ($k = 2$) are due to persistence and period doubling bifurcation, and the rest are higher multiples of the fundamental orbit B. Because $x = 0$ is the boundary between the involved pieces P_B and P_C of the map $P(\cdot)$, the normal PWL continuous map $Q(x)$ with only two domains can be directly applied here, considering that the slopes in these domains ($\mathcal{D}_B$ and $\mathcal{D}_C$) are $\alpha_1 = \lambda_2$ and $\alpha_2 = \lambda_1\lambda_2$ respectively (and in this case $\mu = P_B(0) = P_C(0) = 1 + \tau(1 - \lambda_2)$).

The generic expressions of fixed points $x^*_{B^{k-1}C}(j, k)$ belonging to $B^{k-1}C/b^{k-1}c$ (j being the index of the point and k the period) can be obtained from the closed set of k equations: $P_B\left(x^*_{B^{k-1}C}(j, k)\right) = x^*_{B^{k-1}C}(j + 1, k)$ ($j = 1 \ldots k - 1$) and $P_C\left(x^*_{B^{k-1}C}(k, k)\right) = x^*_{B^{k-1}C}(1, k)$ (or rearranging (14)). The result is

$$x^*_{B^{k-1}C}(j, k) = \frac{1 - \lambda_2\,(1 - \lambda_1)\left(1 - \lambda_2^{k-j}\right)(1 + \tau\,(1 - \lambda_2))}{(1 - \lambda_2)(1 - \lambda_1\lambda_2^k)}. \tag{28}$$

The existence of higher period orbits with $k > 2$ requires the condition $0 < \lambda_2 < 1$. Moreover, there is

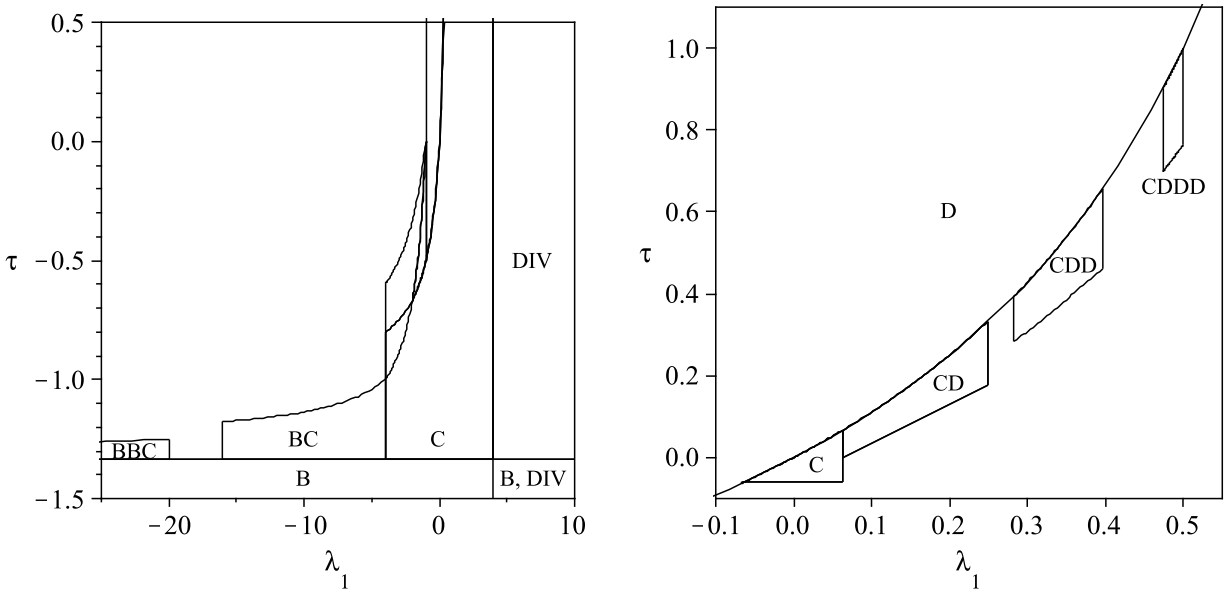

Fig. 12. Analytically obtained 2-D bifurcation diagrams showing parameter regions for stable orbits of type: (a) $B^{k-1}C$ with fixed parameter $\lambda_2 = 0.25$ as in Fig. 10(c) and (b) $CD^{k-1}C$ with fixed parameter $\lambda_2 = -16$.

no limit for k-periodic orbits whenever condition $0 < \lambda_2 < 1/2$ is fulfilled. To prove these results we use the generic conditions of existence and stability of k-periodic orbits in (13) taking into account the relations between α_1, α_2 and λ_1, λ_2 and the corresponding fixed point expressions (14).

The critical slope values for existence and stability are

$$\lambda_{CrExB^{k-1}C} = -\frac{\lambda_2^{1-k} - 1}{1 - \lambda_2}, \tag{29}$$

$$\lambda_{CrStB^{k-1}C} = -\lambda_2^{-k}. \tag{30}$$

If the slope $\lambda_2 > 0$, a generic orbit of the form $B^{k-1}C$ can exist and it is stable if $\lambda_{CrStB^{k-1}C} < \lambda_1 < \lambda_{CrExB^{k-1}C}$. On the contrary, if $\lambda_2 < 0$, existence and stability of $B^{k-1}C$ require $\lambda_{CrExB^{k-1}C} < \lambda_1 < \lambda_{CrStB^{k-1}C}$. Two additional existence conditions are related to the parameter τ

$$\tau > -\frac{1}{1 - \lambda_2}, \tag{31}$$

$$\tau < -\frac{\left(1 - \lambda_2^k\right)\lambda_1}{\left(1 - \lambda_2\right)\left(1 - \lambda_1\right)}. \tag{32}$$

The first one is due to the requirement that the curves of the map in the domains $\mathcal{D}_B$ and $\mathcal{D}_C$ intersect at a positive phase ($P(0) = 1 + (1 - \lambda_2)\tau > 0$). The second one implies that the latest fixed point ($x^*_{B^{k-1}C}(k,k)$) must be located in the curve corresponding to the domain $\mathcal{D}_C$, so the boundary Σ_{CD} must be taken into account ($\lambda_1 x^*_{B^{k-1}C}(k,k) < \tau$).

An interesting fact is the maximum attainable value of the k-periodic orbits of these orbits (with a suitable value of τ). Apart from the trivial case $k = 2$ for $-1 < \lambda_2 < 0$, a more complex situation is given if $0 < \lambda_2 < 1$. In this last case, stable periodic $B^{k-1}C$ orbits requires that $\lambda_{CrStB^{k-1}C} < \lambda_{CrExB^{k-1}C}$. From these restrictions and from (29)-(30), the condition $1 + \lambda_2^{-k}(1 - 2\lambda_2) > 0$ is derived. The conclusion is that there is no limit for k if $0 < \lambda_2 < 1/2$, but if $1/2 < \lambda_2 < 1$, there is an upper limit $k_{MaxB^{k-1}C}$ for k which is

$$k_{MaxB^{k-1}C} = \left\lfloor \frac{\ln\left(2\lambda_2 - 1\right)}{\ln\left(\lambda_2\right)} \right\rfloor, \tag{33}$$

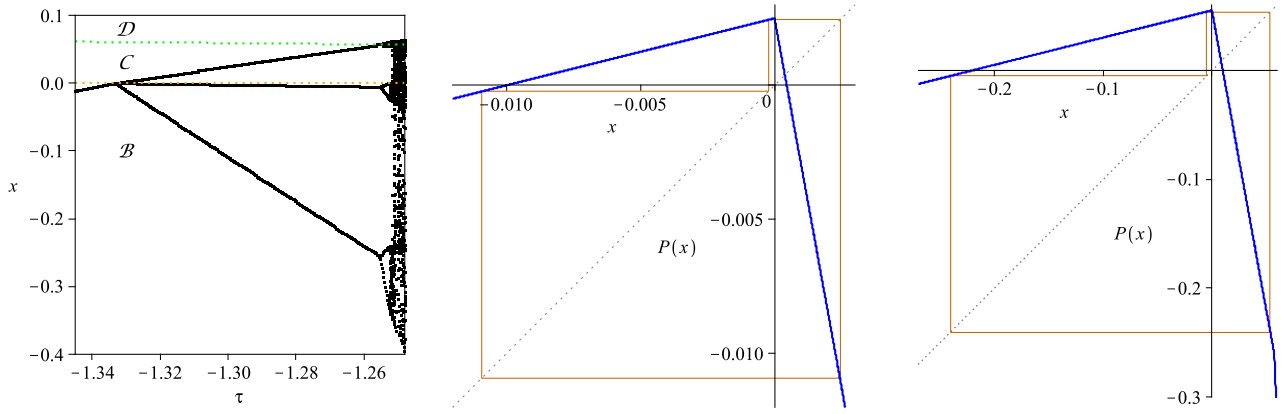

(a) (b) (c)

Fig. 13. (a) Numerically (brute force) obtained 1-D bifurcation diagrams with $\lambda_1 = -22$ and $\lambda_2 = 0.25$ to show B^2C case in Fig. 12(a). Cobweb diagrams with $\tau = -1.33$ (near Σ_{BC} limit) in (b) and $\tau = -1.26$ (near Σ_{CD} limit) in (c).

where $\lfloor \cdot \rfloor$ stands for the floor function. In Fig. 12(a), which is an extension of Fig. 10(c) in order to show additional members of $B^{k-1}C$ series, the k-periodic orbits are not limited because $\lambda_2 = 0.25 < 0.5$ (members up to $k = 3$ have been represented). Notice that in the region of the parameter space represented, where $\lambda_1\lambda_2 > 1$, there is divergence[2] (coexisting with the orbit B if admissible). A 1-D bifurcation diagram in Fig. 13(a) illustrates the limits of the orbit B^2C, which connects to B at the boundary Σ_{BC} and to the orbit B^2CB^2D at the boundary Σ_{CD} (period doubling in this case).

The cobweb diagrams in Fig. 13(b) and 13(c) show a periodic behavior corresponding to the orbit B^2C near the boundaries Σ_{BC} and Σ_{CD} respectively.

4.7.2. *The series of type CD^{k-1}/cd^{k-1}*

These orbits are equivalent to $B^{k-1}C$ due to symmetry. Consequently similar diagrams than in Fig. 12(a) can be obtained with parameter λ_1 fixed instead of λ_2. However, let us show here the complementary diagrams still maintaining λ_2 as the fixed parameter. In this case, stable CD^{k-1} series has finite members and requires the condition $\lambda_2 < -1$ to be fulfilled. The normal PWL 1-D map with two domains can also be used under these considerations: the slopes of the involved pieces P_C and P_D are $\lambda_1\lambda_2$ and λ_1 respectively and the boundary to be applied is now between domains $\mathcal{D}_C$ and $\mathcal{D}_D$ ($\Sigma_{CD} \equiv \lambda_1 x - \tau = 0$), which maps to $1 + \tau$. The critical value $\lambda_{CrExCD^{k-1}}$ of the parameter λ_1 concerning existence can be obtained as a root of the following polynomial in z

$$1 - \lambda_2 - z^{1-k} + \lambda_2 z, \tag{34}$$

and concerning stability, the critical value $\lambda_{CrStCD^{k-1}}$ is defined as

$$\lambda_{CrStCD^{k-1}} = (-\lambda_2)^{-1/k}. \tag{35}$$

The conditions of existence and stability can be summarized as: $\lambda_{CrExCD^{k-1}} < \lambda_1 < \lambda_{CrStCD^{k-1}}$. Therefore, the condition $\lambda_{CrExCD^{k-1}} < \lambda_{CrStCD^{k-1}}$ must hold in order to find stable periodic orbits type CD^{k-1}, so the periodicity is restricted to $k \leq \lfloor k_{MaxCD^{k-1}} \rfloor$, where the critical value $k_{MaxCD^{k-1}}$ is obtained by imposing the equality $\lambda_{CrExCD^{k-1}} = \lambda_{CrStCD^{k-1}}$ which results in

$$k_{MaxCD^{k-1}} = -\frac{\ln(-\lambda_2)}{\ln\left(\frac{1}{2}\left(1 + \frac{1}{\lambda_2}\right)\right)} \tag{36}$$

[2]It is worth noting that divergence is possible mathematically but not physically due to restrictions on some parameters as mentioned previously.

Concerning the parameter τ, its maximum value is obtained from the boundary Σ_{CD} applied to the former orbit D, so the inequality $\tau < \tau_{C\leftrightarrow D}$ is a necessary existence condition, where $\tau_{C\leftrightarrow D}$ is defined in (20). The expression of the minimum value of the parameter τ is specific for each CD^{k-1} member and it is obtained by forcing the first fixed point ($x^*_{CD^{k-1}}(1,k) \in \mathcal{D}_D$) to collide with the boundary Σ_{AD} ($x = 0$), thus resulting in the following expression

$$\tau > \frac{\lambda_1\left(1+\lambda_2\left(\lambda_1^{k-1}-1\right)\right)-1}{(1-\lambda_1)(1-\lambda_2)}. \tag{37}$$

In the 2-D bifurcation diagram in Fig. 12(b), the limits of stable CD^{k-1} orbits have been represented in the parameter space (λ_1, τ) with $\lambda_2 = -16$. In this case, $k_{MaxCD^{k-1}} = 4.38$, so $k = 4$ is the maximum period.

4.7.3. *The series of type $A^{k-1}C/a^{k-1}c$*

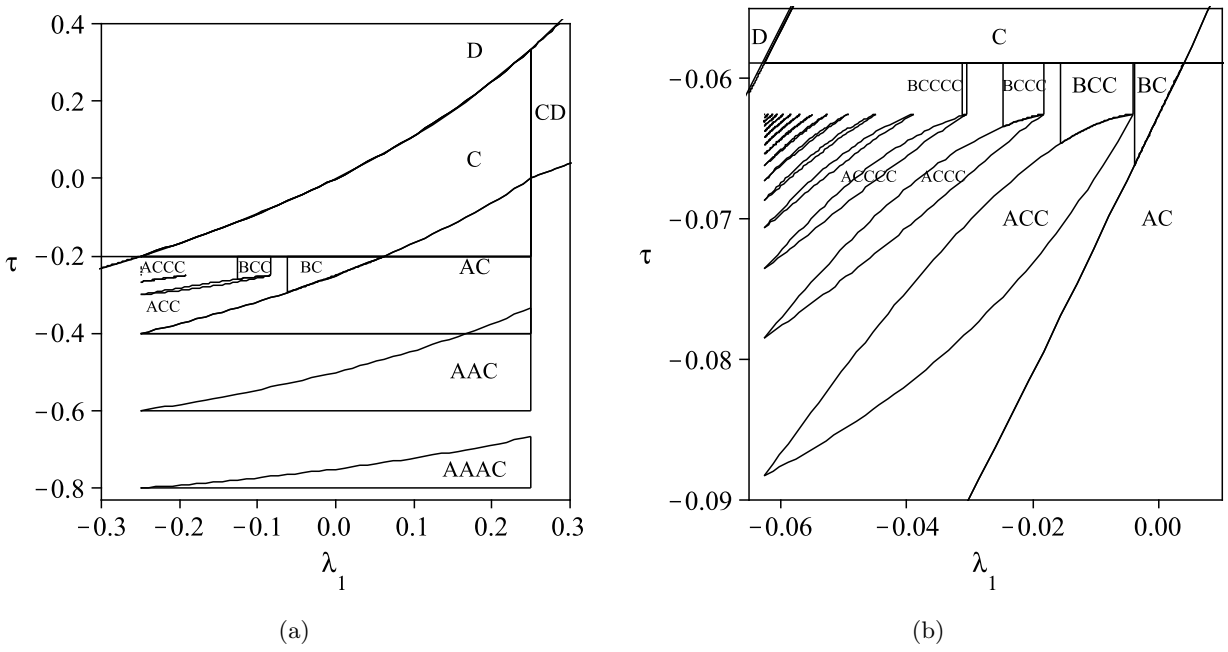

Fig. 14. 2-D analytically obtained bifurcation diagrams for stable orbits: $A^{k-1}C$ with $\lambda_2 = -4$ (as in Fig. 10(a)) and (b) AC^{k-1} and BC^{k-1} with $\lambda_2 = -16$.

Following a similar procedure than above, the k different particular points $x^*_{A^{k-1}C}(j,k)$ of generic member $A^{k-1}C/a^{k-1}c$ take the following form

$$x^*_{A^{k-1}C}(j,k) = j + \frac{k\lambda_1\lambda_2 + \tau(1-\lambda_2)}{1-\lambda_1\lambda_2}, \quad j = 1\ldots k. \tag{38}$$

The members with $j = 1\ldots k-1$ correspond to points located in the domain $\mathcal{D}_A$ while the last k member belongs to the domain $\mathcal{D}_C$. It should be noticed that A and C are non-consecutive partitions of the map. Taking into account the unitary slope in the domain $\mathcal{A}$, the stability condition is equivalent for all $A^{k-1}C$ orbits (including the trivial case C): $|\lambda_1\lambda_2| < 1$. The existence conditions, considering $\tau < 0$, are given by $x^*_{A^{k-1}C}(k-1,k) < \tau$ and $x^*_{A^{k-1}C}(k,k) > 0$ (corresponding to the boundaries Σ_{AB} and Σ_{BC} respectively)

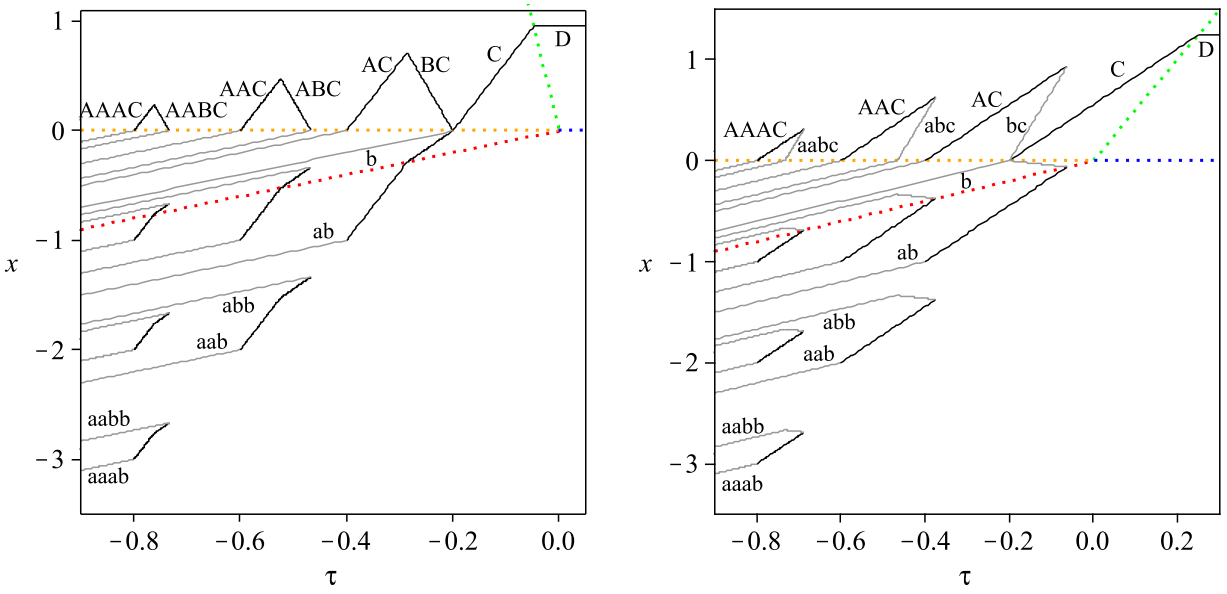

Fig. 15. Analytically obtained 1-D bifurcation diagrams for sections in Fig. 14(a) ($\lambda_2 = -4$) with (a) $\lambda_1 = -0.05$ and (b) $\lambda_1 = 0.2$.

and take the form

$$\tau < \frac{k-1+\lambda_1\lambda_2}{\lambda_2(1-\lambda_1)} \equiv \tau_{A^{k-1}C \leftrightarrow A^{k-2}BC}, \tag{39}$$

$$\tau > -\frac{k}{1-\lambda_2} \equiv \tau_{A^{k-1}C \leftrightarrow A^{k-1}B}. \tag{40}$$

The orbit $A^{k-1}C/a^{k-1}c$ exists if $\tau_{A^{k-1}C \leftrightarrow A^{k-1}B} < \tau < \tau_{A^{k-1}C \leftrightarrow A^{k-2}BC}$ and therefore, $\tau_{A^{k-1}C \leftrightarrow A^{k-2}BC} - \tau_{A^{k-1}C \leftrightarrow A^{k-1}B}$ must be positive. Taking into account that $\lambda_1 < 1$, $\lambda_2 < -1$, $\lambda_1\lambda_2 > -1$ and

$$\tau_{A^{k-1}C \leftrightarrow A^{k-2}BC} - \tau_{A^{k-1}C \leftrightarrow A^{k-1}B} = \frac{(k-1+\lambda_2)\,(1-\lambda_1\lambda_2)}{\lambda_2\,(1-\lambda_1)\,(1-\lambda_2)}, \tag{41}$$

periodicity is restricted to $k \leq \lfloor k_{MaxA^{k-1}C} \rfloor$, where

$$k_{MaxA^{k-1}C} = 1 - \lambda_2. \tag{42}$$

Moreover, the orbits $A^{k-1}C$ and A^kC coexist if $\tau_{A^kC \leftrightarrow A^{k-1}BC} > \tau_{A^{k-1}C \leftrightarrow A^{k-1}B}$, giving the condition: $k(1-\lambda_1\lambda_2)+\lambda_1\lambda_2(1-\lambda_2) < 0$. If in addition the most favorable case for coexistence $\lambda_1\lambda_2 = 1$ is considered, the coexistence is given, in the appropriate range for parameters λ_1 and τ, if $k \leq \lfloor k_{MaxCo(A^{k-1}C,A^kC)} \rfloor$, where

$$k_{MaxCo(A^{k-1}C,A^kC)} = \frac{1-\lambda_2}{2}. \tag{43}$$

The regions in the parameter space (λ_1, τ) for (stable) $A^{k-1}C$ orbits have been depicted in Fig. 14(a) with $\lambda_2 = -4$. In this case, $k_{MaxA^{k-1}C} = 5$ (highest period $k = 5$ is a limit case with $\tau_{A^{k-1}C \leftrightarrow A^{k-2}BC} - \tau_{A^{k-1}C \leftrightarrow A^{k-1}B} = 0$) and $k_{MaxCo(A^{k-1}C,A^kC)} = 2.5$ so there is coexistence between cases $k = 1$ and $k = 2$ from one side and between $k = 2$ and $k = 3$ from another side.

To give details about other orbits related to these series, a pair of 1-D bifurcation diagrams taking τ as a bifurcation parameter have been represented in Fig. 15. These orbits are $A^{k-2}BC/a^{k-2}bc$, $a^{k-1}b$ and $a^{k-2}b^2$. In Fig. 15(a) with $\lambda_1 = -0.05$, $A^{k-2}BC$ is stable ($\lambda_1\lambda_2^2 = -0.8$) so there is persistence between $A^{k-1}C$ and $A^{k-2}BC$ at Σ_{AB}. However, in Fig. 15(b) with $\lambda_1 = 0.2$, $a^{k-2}bc$ is unstable ($\lambda_1\lambda_2^2 = 3.2$) so there is a saddle node or fold bifurcation involving $A^{k-1}C$ and $a^{k-2}bc$ at Σ_{AB}. The coexistence between C and AC and also between AC and A^2C can be observed in this last case.

4.7.4. *The series of type BC^{k-1}/bc^{k-1}*

These orbits are also examples of k-periodic orbits ($k > 1$) from a former orbit (C in this case). An illustrative example of them and the related AC^{k-1} orbits is in Fig. 14(b). Actually, the orbits BC^{k-1} orbits are defined in only two connected domains, so the results concerning the 1-D PWL continuous map $Q(X)$ with two domains can be applied. These domains are $\mathcal{D}_B$ (with $\alpha_1 = \lambda_2$) and $\mathcal{D}_C$ ($\alpha_2 = \lambda_1\lambda_2$) connected at Σ_{BC}. The stable BC^{k-1} members are found in the parameter domain $\lambda_2 < -1$ and $0 < \lambda_1\lambda_2 < 1$. Regarding these slopes, the existence and stability conditions can be summarized as $\lambda_{CrStBC^{k-1}} < \lambda_1 < \lambda_{CrExBC^{k-1}}$, where $\lambda_{CrExBC^{k-1}}$ is a root of the following polynomial in z

$$(1 + \lambda_2)z^{k-1} - z^{k-2} - \lambda_2^{1-k}, \tag{44}$$

and

$$\lambda_{CrStBC^{k-1}} = \frac{1}{\lambda_2}\left(\frac{-1}{\lambda_2}\right)^{\frac{1}{k-1}}. \tag{45}$$

Taking into account that the condition $\lambda_{CrStBC^{k-1}} < \lambda_{CrExBC^{k-1}}$ must be fulfilled, the period of the stable orbit BC^{k-1}must be smaller than or equal to $\lfloor k_{MaxBC^{k-1}} \rfloor$, where

$$k_{MaxBC^{k-1}} = 1 + \frac{\ln(-\lambda_2)}{\ln\left(2 + \frac{1}{\lambda_2}\right)}. \tag{46}$$

Concerning the parameter τ, the series BC^{k-1}/bc^{k-1} emerges after C collides with the boundary Σ_{BC}. Moreover, orbits type AC^{k-1} that will be analyzed below are given after the fixed point in $\mathcal{D}_B$ that belongs to BC^{k-1}/bc^{k-1} collides with the boundary Σ_{AB}. To sum up, BC^{k-1}/bc^{k-1} exists if, in addition to the slope conditions, $\tau_{AC^{k-1}\leftrightarrow BC^{k-1}} < \tau < \tau_{B\leftrightarrow C}$, where

$$\tau_{AC^{k-1}\leftrightarrow BC^{k-1}} = \frac{(\lambda_1\lambda_2)^k - 1}{\lambda_2\,(1 - \lambda_1)\left((\lambda_1\lambda_2)^{k-1} - 1\right)}. \tag{47}$$

4.7.5. *The series of type AC^{k-1}/ac^{k-1}*

The orbits AC^{k-1}/ac^{k-1} are related to the orbits BC^{k-1}/bc^{k-1} as mentioned above (Fig. 14(b)). In this case, $\alpha_1 = 1$ and $\alpha_2 = \lambda_1\lambda_2$, and therefore, the stability condition is $\lambda_1\lambda_2 < 1$ (members $k > 2$ of these series are restricted to negative values of λ_1 and λ_2 slopes). In the parameter space (λ_1, τ), the existence of AC^{k-1} is delimited by two lines that intersect at two codimension-2 points: $(\lambda_2^{-1}, -k(k-1)^{-1}(1-\lambda_2)^{-1})$ and $(\lambda_{CrExBC^{k-1}}, \lambda_2^{-1})$. Besides, the upper limit of τ coincides with the lower limit $\tau_{AC^{k-1}\leftrightarrow BC^{k-1}}$ obtained for BC^{k-1}/bc^{k-1} orbits and the lower limit stands for k-fixed point (in $\mathcal{D}_C$) colliding at Σ_{BC}. Existence conditions regarding τ can therefore be summarized as $\tau_{AC^{k-1}\leftrightarrow AC^{k-2}B} < \tau < \tau_{AC^{k-1}\leftrightarrow BC^{k-1}}$, where

$$\tau_{AC^{k-1}\leftrightarrow AC^{k-2}B} = \frac{(\lambda_1\lambda_2)^{k-2}\,(1 - 2\lambda_1\lambda_2) + 1}{(1 - \lambda_2)\left((\lambda_1\lambda_2)^{k-1} - 1\right)}. \tag{48}$$

The period k is limited by the fact that codimension-2 points cannot go further than the point $(\lambda_2^{-1}, \lambda_2^{-1})$ defined by lines $\lambda_1 = \lambda_2^{-1}$ and $\tau = \lambda_2^{-1}$. Taking into account the lower-left points, the inequality $-k(k-1)^{-1}(1-\lambda_2)^{-1} \leq \lambda_2^{-1}$ is obtained, and from it: $k \leq \lfloor k_{MaxAC^{k-1}} \rfloor$, where

$$k_{MaxAC^{k-1}} = 1 - \lambda_2. \tag{49}$$

5. Dynamics from the continuous-time switched model and discussion

In order to verify the analytical results and to have a more general view including other complex dynamics, 2-D bifurcation diagrams in Fig. 16(a) (related to Fig. 12(a) with $\lambda_2 = 0.25$) and in Fig. 16(b) (with $\lambda_1 = 0.25$) have been obtained by iterations of map $P(x)$. Each color corresponds to a specific periodic

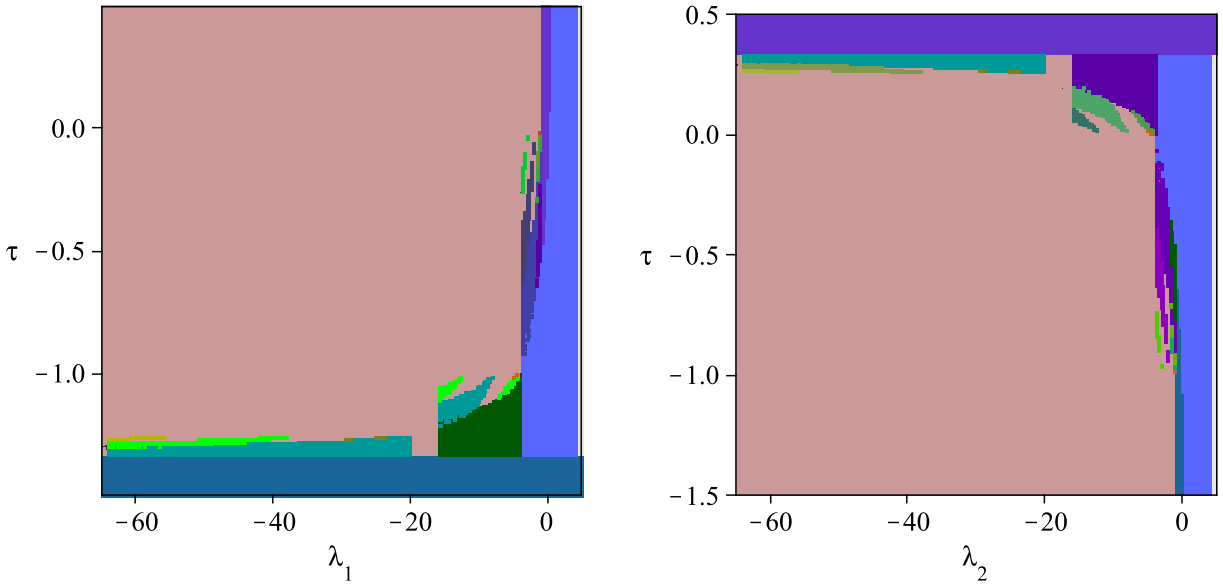

Fig. 16. Numerically obtained 2-D bifurcation diagrams with colored regions for the different periodic orbits obtained by brute force methods applied to map $P(x)$. The fixed parameter is $\lambda_2 = 0.25$ (as in Fig. 12(a)) in (a) and it is $\lambda_1 = 0.25$ in (b). Symmetry of the map is clearly observed (considering the orbit equivalence).

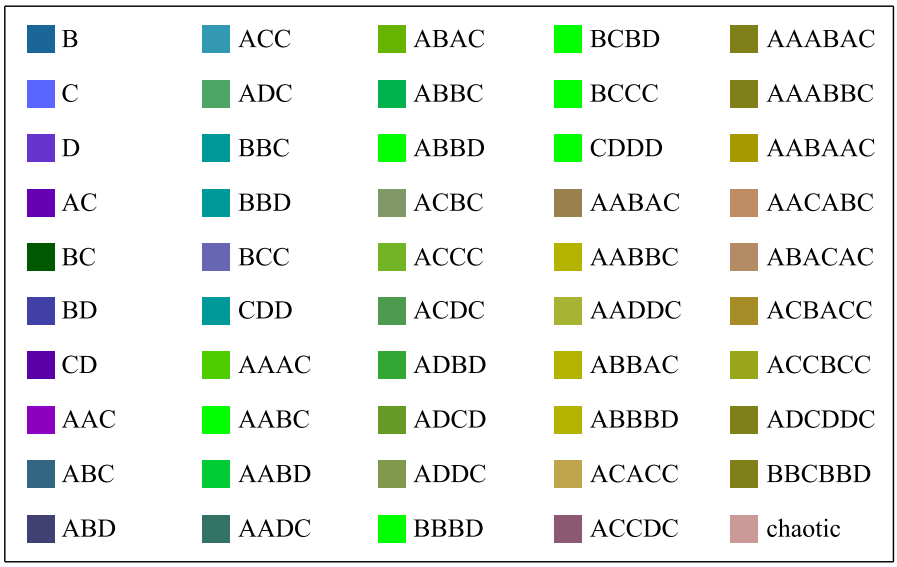

Fig. 17. Color-code for the more relevant orbits in the 2-D bifurcation diagrams.

orbit, except the pink area that corresponds to chaotic dynamics. The color-code for all the 2-D bifurcation diagrams presented in this paper is shown in Fig. 17.

In Fig. 16(b), the upper region corresponds to D case and below it, there are members of CD^{k-1} series (from right to left C, CD and CD^2). Furthermore, below the orbit C, the members of $A^{k-1}C$ series appear and the same scheme is repeated below the orbit DC (the series of type $A^{k-2}DC$). Complementary diagram in Fig. 16(a) has been plotted to show up the symmetric properties of the map. In this case, B corresponds to the bottom area and above (from right to left) C, BC and BC^2 appear.

The bifurcation diagram in Fig. 18(a) has been plotted for $\lambda_2 = -4$, thus corresponding to Fig. 10(a)

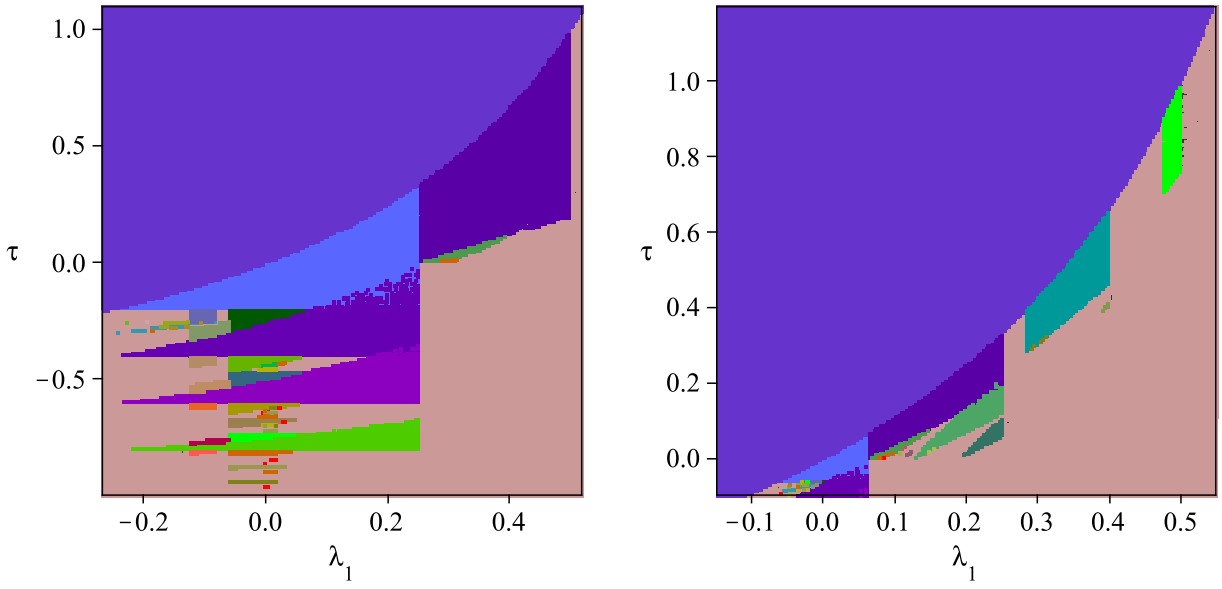

Fig. 18. Color-coded numerically obtained 2-D bifurcation diagrams. The fixed parameter is $\lambda_2 = -4$ (as Fig. 10(a)) in (a) and it is $\lambda_2 = -16$ (as Fig. 12(b)) in (b).

and Fig. 14(a). The upper area refers to D, which is merged (from left to right) to C and CD. In turn, the orbit C is the lower member of the $A^{k-1}C$ series. The series BC^{k-1} and AC^{k-1} take place (in the left side between C and AC. Other related orbits, manifesting themselves as additive or multiple sequences, appear in the diagram mainly in the central region between consecutive AC^{k-1} members. The analysis of these and other complex orbits is out of the scope of this paper.

The bifurcation diagram in Fig. 18(b) with $\lambda_2 = -16$ corresponds to Fig. 12(b) giving successive CD^{k-1} orbits. A series $A^{k-2}DC$, starting by DC, with coexistence between DC and ADC in a similar manner than simpler $A^{k-1}C$ series, can be observed.

Direct simulation of the circuit gives the top and the middle 1-D bifurcation diagrams by varying the parameter $V_2 = V_{LN}$ (in order to vary the normalized τ) in Fig. 19. These diagrams have been plotted with physical parameters, given in the caption, that fit normalized $\lambda_2 = -4$ in Fig. 18(a) and the points have been represented for a fixed parameter, given in the figure caption, after the steady state is reached. The diagrams on the left correspond to $V_P = 8.4\,\mathrm{V}$ (normalized $\lambda_1 = -0.05$) thus showing the series $A^{k-1}C$ without coexistence, but with persistence to the intermediate orbits $A^{k-2}BC$. Furthermore, finite sequence of period doubling of these last orbits leading to chaos is observed. The middle and right diagrams correspond to $V_P = 6.4\,\mathrm{V}$ (normalized $\lambda_1 = 0.2$) and have been plotted by sweeping the bifurcation parameter from left to right (middle diagrams) and right to left (right diagram) in order to show coexistence of C with AC and AC with AC^2. The top diagrams have been represented with physical variables and the middle ones using dimensionless normalized variables. To validate the 1-D PWL continuous map $P(x)$, the bottom diagrams have been obtained by iterations of map $P(x)$. A perfect match can be observed in these diagrams and with analytical results from the 1-D PWL continuous map $P(x)$ given in Fig. 15.

Finally, the control signal $r_S i_L$ and ramps (v_{rP} and v_{rN}) in steady state have been represented in two oscillogram series in Fig. 20. The top diagrams use the same parameters than in Fig. 19(a) besides $V_{LN} = 2.71\,\mathrm{V}$ ($\tau = -0.15$) in Fig. 20(a), $V_{LN} = 2.65\,\mathrm{V}$ ($\tau = -0.25$) in Fig. 20(b), and $V_{LN} = 2.59\,\mathrm{V}$ ($\tau = -0.35$) in Fig. 20(c). These parameter sets have been chosen to illustrate the behavior corresponding to the orbits C, BC and AC respectively. The bottom diagrams use parameters in 19(b) besides $V_{LN} = 2.8\,\mathrm{V}$ ($\tau = 0$) in Fig. 20(d), and $V_{LN} = 2.74\,\mathrm{V}$ ($\tau = -0.1$) in Figs. 20(e) and 20(f). Appropriate initial conditions have been used to obtain both coexisting solutions.

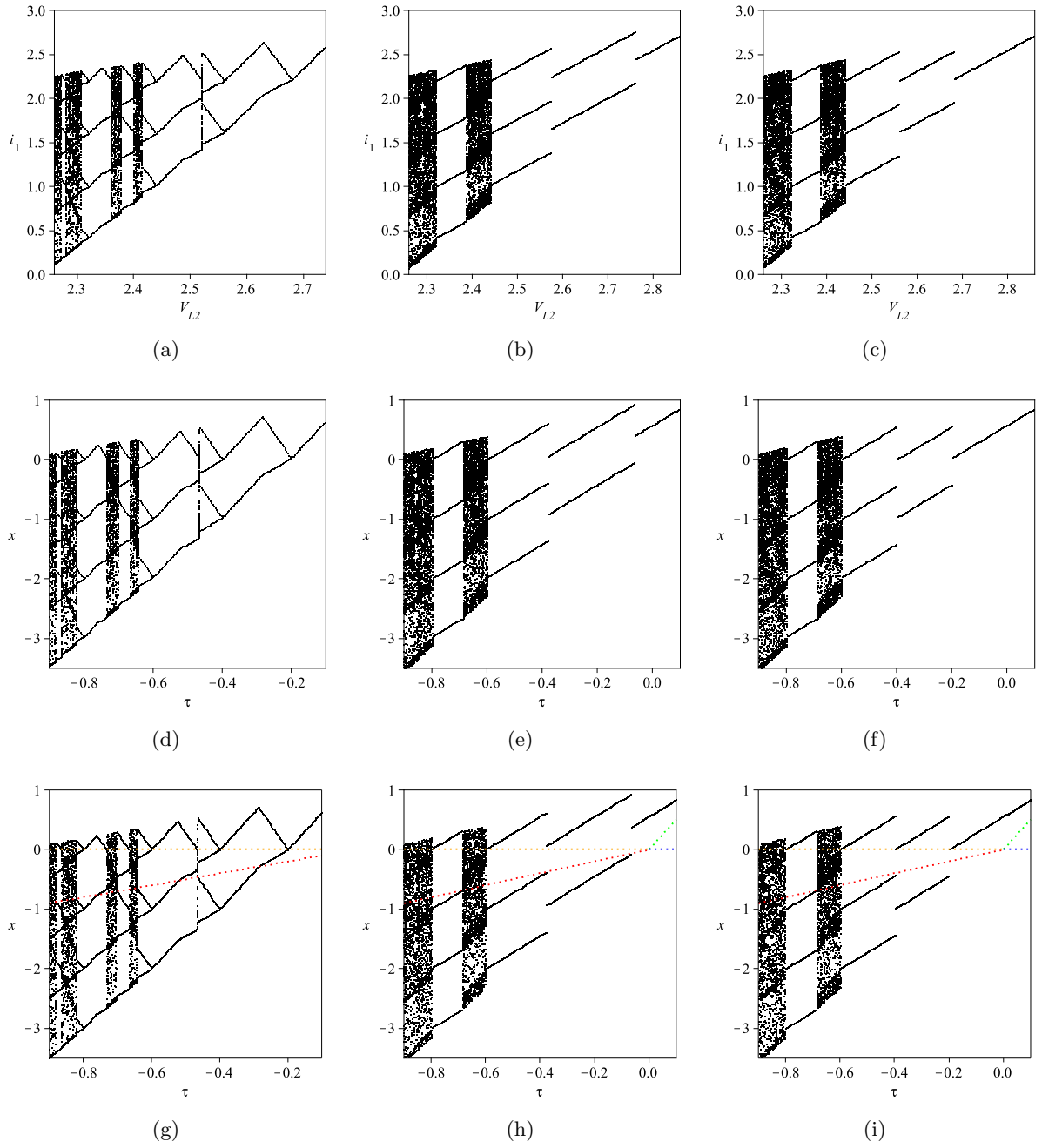

Fig. 19. 1-D bifurcation diagrams obtained from direct simulation of the circuit with physical variables and parameters (up) and normalized ones (center), and from the 1-D PWL continuous map $P(x)$ (bottom). Parameters: $V_g = 3\,\mathrm{V}$, $L = 10\,\mu\mathrm{H}$, $r_S = 1\,\Omega$, $V_N = -37\,\mathrm{V}$ (normalized $\lambda_2 = -4$), $V_R = 1\,\mathrm{V}$, $T = 2\,\mu\mathrm{s}$, $\phi = 0.5$, $V_{LP} = 2.5\,\mathrm{V}$. Besides, $V_P = 8.4\,\mathrm{V}$ ($\lambda_1 = -0.05$) on left diagrams and $V_P = 6.4\,\mathrm{V}$ ($\lambda_1 = 0.2$) on center and right diagrams (made from left to right and vice verse). A perfect agreement between numerical simulations and map iterations and also with analytical results from the map in Fig. 15 can be observed.

Conclusion

Single-Inductor Multiple-Output (SIMO) converters are suitable switched mode power conversion circuits for applications where different output voltages must be stabilized to their respective references. In this paper a Single-Inductor Two-Output (SITO) DC-DC converter with PWM interleaved control has been studied. Under the tight regulation condition of the output voltages, the dynamical behavior of this system can be described by a 1-D PWL map with four domains and three dimensionless parameters. The

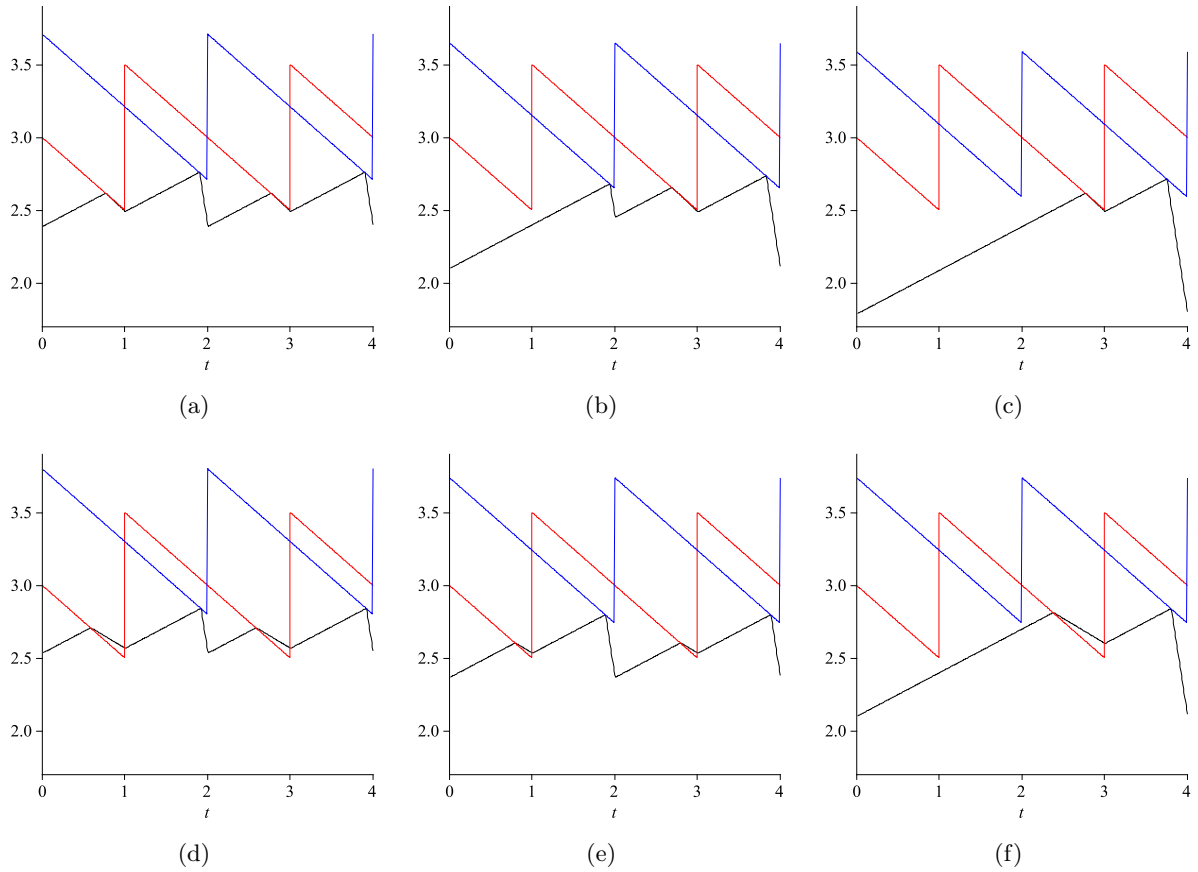

Fig. 20. Control signals $r_S i_L$, v_{rP} and v_{rN} waveforms (black, red and blue color respectively). Time is in μs and signals are in V. Parameters are those in Fig. 19 with $V_P = 8.4\,\mathrm{V}$ ($\lambda_1 = -0.05$) and $V_{LN} = 2.71\,\mathrm{V}$ ($\tau = -0.15$) in (a), $V_{LN} = 2.65\,\mathrm{V}$ ($\tau = -0.25$) in (b) and $V_{LN} = 2.59\,\mathrm{V}$ ($\tau = -0.35$) in (c), and with $V_P = 6.4\,\mathrm{V}$ ($\lambda_1 = 0.2$) and $V_{LN} = 2.8\,\mathrm{V}$ ($\tau = 0$) in (d) and $V_{LN} = 2.74\,\mathrm{V}$ ($\tau = -0.1$) in (e,f). Oscillogram correspond to C in (a), (d) and (e), BC in (b) and AC in (c) and (f). Notice that the same parameters are used in (e) and (f), so orbits C and AC coexist (different initial conditions have been used to obtain both limit solutions).

non-smooth bifurcation behavior of this map has been studied both analytically and by using numerical simulations. Different bifurcation patterns have been unfolded in a wide range of the parameter space using 1-D and 2-D bifurcation diagrams. The expression of the different k-periodic solutions, their domain of existence and their stability have been obtained in closed form. Coexistence of more than two solutions in some regions of the parameter space has been also studied. The chart of dynamical behavior in the parameter space for this system has been obtained through a detailed analytical study and validated by numerical simulations. We have shown that, under parameter variation, the desired 1-periodic regime undergoes different non-smooth bifurcation, where a k-periodic orbit or chaotic orbit arises according to some specific and established patterns. Different scenarios have been detected for losing the stability of a certain 1-periodic orbit. Numerical simulations from the 1-D piecewise model and from the circuit-based switched model validate the analytical results. It is important to note that the phenomena observed are not restricted to the system under study, but can occur in more complex SIMO converters and in many other physical systems that can be described with PWL continuous maps.

Acknowledgments

This work was partially supported by the Spanish *Ministerio de Educación e Innovación* under grant DPI2010-16481.

References

Banerjee, S., Yorke J. A and Grebogi, C. [1998] "Robust chaos," *Physics Review Letters*, 80:3049-3052.

Banerjee, S., Karthik, M. S., Yuan, G. and Yorke J. A. [2000a] "Bifurcations in One-Dimensional Piecewise Smooth Maps-Theory and Applications in Switching Circuits," *IEEE Transactions on Circuits and Systems - I*, 47(3):389-394.

Banerjee, S. Ranjan, P. and Grebogi, C. [2000b] "Bifurcations in Two-Dimensional Piecewise Smooth Maps-Theory and Applications in Switching Circuits," *IEEE Transactions on Circuits and Systems - I*, 47(5):633-643.

Banerjee, S. and Verghese, G. C. [2001] *Nonlinear Phenomena in Power Electronics: Bifurcations, Chaos, Control and Applications.* Wiley - IEEE Press, New York.

Benadero, L., El Aroudi, A., Giral, R. and Calvente, J. [2006] "Stability analysis of a single inductor dual switching DC-DC converter," *Mathematics and Computers in Simulation*, 71(4-6):256-269.

Benadero, L., Moreno-Font, V., El Aroudi, A. and Giral, R. [2008] "Single inductor multiple outputs interleaved converters operating in CCM," In *Proc. 13th Power Electronics and Motion Control Conference (EPE-PEMC)*, Poznan, Poland.

Benadero, L., Moreno-Font, V., El Aroudi, A. and Giral, R. [2011] "Topologies and control of a class of single inductor multiple-output converters operating in continuous conduction mode," *IET Power Electronics*, 4(8):927-935.

Botella-Soler, V. Oteo, J. A. and Ros J. [2012] "Coexistence of periods in a bifurcation," *Chaos, Solitons and Fractals*, 45:681-686.

Buti, B., Nagy, I. and Masada, E. [2006] "Stability analysis of PWM-controlled dual channel resonant buck and boost converter using PI controller," In *12th International Power Electronics and Motion Control Conference*, 1:869-876.

Deane, J. H. B. and Hamill, D. C. [1990] "Analysis, simulation and experimental study of chaos in the buck converter," In *IEEE Power Electronics Specialist Conference (PESC)*, 491-498.

Deane, J. H. B. [1992] "Chaos in a current-mode controlled boost DC-DC converter," *IEEE Transactions on circuits and systems - I*, 39(8):680-683.

Dénes, I. and Nagy, I. [2003] "Two models for the dynamic behavior of a dual-channel buck and boost DC-DC converter," *Electromotion*, 10(4):556-561.

di Bernardo, M., Budd, C. J. and Champneys, A. R. [1998] "Grazing, skipping and sliding: analysis of the non-smooth dynamics of the dc/dc buck converter," *Nonlinearity*, 11(4):859-890.

di Bernardo, M., Garofalo, F., Glielmo, L. and Vasca, F. [1998] "Switchings, bifurcations and chaos in dc/dc converters," *IEEE Transactions on Circuits and Systems - I*, 45(2):133-141.

di Bernardo, M. and Vasca, F. [2000] "Discrete-time maps for the analysis of bifurcations and chaos in dc/dc converters," *IEEE Transactions on Circuits and Systems - I*, 47(2):130-173.

di Bernardo, M., Budd, C., Champenys, A. and Kowalczyk, B. [2008] *Piecewise-Smooth Dynamical Systems: Theory and Applications.* Springer-Verlag.

El Aroudi, A., Benadero, L., Toribio, E. and Machiche, S. [2000] "Quasiperodicity and chaos in the DC-DC buck-boost converter," *International Journal of Bifurcation and Chaos*, 10(2):359-371.

El Aroudi, A., Debbat, M., Olivar, G., Benadero, L., Toribio, E. and Giral, R. [2005] "Bifurcations in DC-DC switching converters: Review of methods and applications," *International Journal of Bifurcation and Chaos*, 15(5):1549-1578.

El Aroudi, A., Debbat, M. and Martinez-Salamero, L. [2007] "Poincaré maps modeling and local orbital stability analysis of discontinuous piecewise affine periodically driven systems," *Nonlinear Dynamics*, 50(3):431-445.

El Aroudi, A., Moreno-Font, V. and Benadero, L. [2009] "Dynamical analysis of an interleaved single inductor TITO switching regulator," *Mathematical Problems in Engineering*, 2009 (Article ID 946245):19 pages.

El Guezar, F., Bouzahir, H. and Fournier-Prunaret, D. [2011] "Event detection occurrence for planar piece-wise affine hybrid systems," *Nonlinear Analysis: Hybrid Systems*, 5(4):626-638.

Erickson, R. W. and Maksimovič, D. [2001] *Fundamentals of Power Electronics.* Springer.

Giaouris, D., Banerjee, S., Imrayed, O., Mandal, K., Zahawi, B. and Pickert, V. [2012] "Complex interaction between tori and onset of three-frequency quasi-periodicity in a current mode controlled boost converter," *IEEE Transactions on Circuits and Systems - I*, 59(1):207-214.

Hamill, D. C., Deane J. H. B. and Jefferies, D. J. [1992] "Modelling of Chaotic DC-DC Converters by Iterated Nonlinear Mapping," *IEEE Transactions on Power Electronics*, 7(1):25-36.

Hamill, D. C. and Jefferies, D. [1988] "Subharmonics and chaos in a controlled switched-mode power converter," *IEEE Transactions on Circuits and Systems - I*, 35(8):1059-1061.

Hamar, J. and Nagy, I. [2003] "Asymmetrical operation of dual channel resonant DC-DC converters," *IEEE Transactions on Power Electronics*, 18(1):83-94.

Iu, H. H. C. and Tse, C. K. [2000] "Bifurcation behavior in parallel-connected buck converters," *IEEE Transactions on Circuits and Systems - I*, 48(2):233-240.

Iu, H. H. C., Tse, C. K. and Dranga, O. [2005] "Bifurcation in parallel-connected buck converters under current-mode control," In *IEEE International Symposium on Circuits and Systems (ISCAS)*, (5):4445-4448.

Kabe, T., Parui, S., Torikai, H., Banerjee, S. and Saito, T. [2007] "Analysis of piecewise constant models of current mode controlled DC-DC converters," *IEICE Transactions on Fundamentals of Electronics, Communication and Computer Sciences*, E90-A(2):448-456.

Ki, W. H. and Ma, D. [2001] "Single-inductor multiple-output switching converters," In *Power Electronics Specialists Conference (PESC)*, (1):226-231.

Kolokolov, Y., Monovskaya, A., Ustinov, P., Essounbouli, N. and Hamzaoui, A. [2011] "Uncertainty of pulse energy conversion system dynamics near bifurcation boundary," *International Journal of Bifurcation and Chaos*, 21(11):3195-3204.

Leine, R. I. and Nijmeijer, H. [2004] *Dynamics and Bifurcations of Non-Smooth Mechanical Systems.* Springer-Verlag.

Ma, D., Ki, W. H., Tsui, C. Y. and Mok, P. K. T. [2001] "A 1.8 V single-inductor dual-output switching converter for power reduction techniques," In *Symposium on VLSI Circuits Digest of Technical Papers*, 137-140.

Ma, D., Ki, W. H., Tsui, C. Y. and Mok, P. K. T. [2003a] "Single-inductor multiple-output switching converters with time-multiplexing control in discontinuous conduction mode," *IEEE Journal of Solid-State Circuits*, 38(1):89-100.

Ma, D., Ki, W. H. and Tsui, C. Y. [2003b] "A pseudo-CCM/DCM SIMO switching converter with freewheel switching," *IEEE Journal of Solid-State Circuits*, 38(6):1007-1014.

Marrero, J. L. R., Font, J. M. and Verghese, G. C. [1996] "Analysis of the chaotic regime for DCDC converters under currentmode control," In *IEEE Power Electronic Specialist Conference (PESC)*, 1477-1483.

Marrero, J. L. R., Bueno, R. S. and Verghese, G. C. [1999] "Analysis and control of chaotic DCDC switching power converters," In *IEEE International Symposium on Circuits and Systems (ISCAS)*, V-287-291.

Mazumder, S. K. [2006] "Stability analysis of parallel DC-DC converters," *IEEE Transactions on Aerospace and Electronic Systems*, 42(1):50-69.

Mohan, N., Undeland, T. M. and Robins, W. P. [2003] *Power Electronics: Converters, Applications and Design.* John Wiley & Sons.

Moreno-Font, V., El Aroudi, A., Benadero, L., Giral, R. and Calvente, J. [2010a] "Dynamics and stability issues of a single inductor dual switching DC-DC converter," *IEEE Transactions on Circuits and Systems - I*, 57(2):415-426.

Moreno-Font, V., El Aroudi, A. and Benadero, L. [2010b] "Modeling and bifurcation behavior of multiphase SIMIMO DC-DC switching regulators," *International Journal of Bifurcation and Chaos*, 20(11):3841-3861.

Moreno-Font V., Benadero, L. and El Aroudi, A. [2011] "Non-Smooth Bifurcations in a 1-D Piecewise Linear Model of a Single - Inductor Two-Output DC-DC Switching Converter," In *IEEE International Symposium on Circuits and Systems (ISCAS)*, 2725-2728.

Nusse, H. E. and Yorke, J. A. [1992] "Border-collision bifurcations including 'period two to period three' for piecewise smooth maps," *Physica D*, 57:39-57.

Nusse E. H., Ott, E. and Yorke, J. A. [1994] "Border-collision bifurcations: An explanation for observed bifurcation phenomena," *Physical Review*, 49(2):48-50

Paolini, E. E., Moiola, J. L., D'Amico, M. B., Angulo, F. and Olivar, G. [2012] "Influence of period-doubling bifurcations in the appearance of border collisions for a ZAD-strategy-controlled buck converter," *International Journal of Circuit Theory and Applications* 40(1):77-91.

Robert, B. and Robert, C. [2002] "Border Collision Bifurcations in a One-Dimensional Piecewise Smooth Map for a PWM Current-Programmed H-Bridge Inverter," *International Journal of Control*, 75(16):1356-1367.

Robert, B. and El Aroudi, A. [2006] "Discrete time model of a multi-cell dc/dc converter: Non linear approach," *Mathematics and Computers in Simulation*, 71(4):310-319.

Saito, T., Kabe, Ishikawa T., Matsuoka, Y. and Torikai, H. [2007] "Piecewise constant switched dynamical systems in power electronics," *International Journal of Bifurcation and Chaos*, 17(10):3373-3386

Tse, C. [1994] "Flip bifurcation and chaos in three-state boost switching regulators," *IEEE Transactions on Circuits and Systems - I*, 41(1):16-23.

Tse, C. K. and Li, M. [2011] "Design-oriented bifurcation analysis of power electronics systems," *International Journal of Bifurcation and Chaos* 21(6):1523-1537.

Yuan, G. Banerjee, S. Ott, E. and Yorke, J. A. [1998] "Border-collision Bifurcations in the Buck Converter," *IEEE Transactions on Circuits and Systems - I*, 45(7):707-716.

Woywode, O., Güldner, H., Baranovski, A. L. and Schwarz, W. [2000] "Design rules aperiodic boost converters," *Int. Power Conversion and Intelligent Motion*, PCIM'00.

Woywode, O., Weber, J., Güldner, H., Baranovski, A. L. and Schwarz, W. [2001] "Qualitative dynamics of the boost converter," In *IEEE International Symposium on Circuits and Systems (ISCAS)*, (2):1720.

Zhang, H., Yang, X. P., Ma, X. K., Zheng, F. [2011] "Theoretical and experimental investigation of bidirectional Hopf bifurcations in cascade DC-DC buck converters," *Mathematics and Computers in Simulation* 82(4):540-557.

Zhang, H., Yang, X.-P., Ma, X.-K., He, B. [2012] "Analysis of limit cycle behavior in DC-DC boost converters," *Nonlinear Analysis: Real World Applications*, 13(5):2049-2062.

Zhusubaliyev, T., Soukhoterin, E. A. and Mosekilde, E. [2003] "Quasiperiodicity and border-collision bifurcations in a DC/DC converter with pulsewidth modulation," *IEEE Transactions on Circuits and Systems - I*, 50(8):1047-1057.

Zhusubaliyev, T. and Mosekilde, E. [2006] "Torus birth bifurcation in a DC/DC converter," *IEEE Transactions on Circuits and Systems - I*, 53(8):1839-1850.